THESIS FOR THE DEGREE OF LICENTIATE OF ENGINEERING

Explosions in urban environments

Modelling of gas explosions and risk of premature shear failure in reinforced concrete structures

FABIO LOZANO

Department of Architecture and Civil Engineering

Division of Structural Engineering

CHALMERS UNIVERSITY OF TECHNOLOGY

Gothenburg, Sweden 2023

Explosions in urban environments:
Modelling of gas explosions and risk of premature shear failure in reinforced concrete structures
FABIO LOZANO

Technical Report No. 2023:8
Thesis for the degree of Licentiate of Engineering
Lic/Architecture and Civil Engineering/Chalmers University of Technology

Department of Architecture and Civil Engineering
Division of Structural Engineering
Concrete Structures
Chalmers University of Technology
SE-412 96 Gothenburg
Sweden
Telephone + 46 (0)31-772 1000

Printed by Chalmers Reproservice
Gothenburg, Sweden 2023

Explosions in urban environments:
Modelling of gas explosions and risk of premature shear failure in reinforced concrete structures

FABIO LOZANO
Department of Architecture and Civil Engineering
Division of Structural Engineering
Concrete Structures
Chalmers University of Technology

Abstract

The risk for accidental gas explosions in urban environments has increased in Sweden in recent years. This is due to densification of existing urban centres and the rise of vehicles powered by alternative fuels. Because of this, blast-resistant design of reinforced concrete (RC) structures may eventually become a common aspect of urban development and structural engineering.

This thesis aims at expanding the knowledge concerning explosion and blast loads in urban environments and the response of RC structures subjected to it. Two key research areas were identified. The first one deals with the strength of vapour cloud explosions (VCEs) on urban roads. The strength of the blast source is a necessary input to predict the blast load generated by VCEs. However, there is much subjectivity and inconsistency today in the determination of the explosion strength, particularly for the conditions on urban roads. This work used computational fluid dynamics (CFD) calculations in combination with the principles of factorial design to determine the expected strength for several explosion scenarios on urban roads and identify the most significant parameters affecting the resulting strength. For the studied scenarios, the explosion strength varied approximately from 2 kPa to 100 kPa. Moreover, the number of vehicles in the transversal direction (i.e., vehicles standing side by side) was found to have the most significant effect on the explosion pressure.

The other area is concerned with the uncertainties related to the failure modes of blast-loaded RC one-way slabs. The motivation behind this research area is the need to prevent brittle shear failure in blast-loaded RC elements. The Monte Carlo method was used to determine the probability of premature shear failure of the blast-loaded slabs considering the uncertainties associated with the materials, geometry, and resistance models. The slabs were initially designed to have a balanced failure (i.e., the resistance to shear and bending failure are theoretically equal). Bending failure was found to be the expected failure mode for the studied cases. However, the likelihood of shear failure (particularly for slabs without stirrups) may still be considered relatively high, depending on the risk tolerability of a given design. Thus, an additional partial factor to enhance the confidence level regarding the preferred failure mode was put forward.

Keywords: Vapour cloud explosions, urban road environments, blast strength, blast loading, computational fluid dynamics, factorial design, premature shear failure, model uncertainty, Monte Carlo method

To my parents

& Linnéa

Preface

The research work presented in this Licentiate Thesis is part of a PhD project at the Division of Structural Engineering at Chalmers University of Technology. The study was supported financially by *Trafikverket* (Swedish Transport Administration, Sweden), *Fortifikationsverket* (Swedish Fortifications Agency, Sweden) and *Myndigheten för samhällsskydd och beredskap* (Swedish Civil Contingencies Agency, Sweden). The work was conducted between February 2021 and August 2023. The PhD project is part of a larger collaboration project between the Division of Structural Engineering at Chalmers and the Division of Concrete Structures at KTH, entitled *Explosions in Densified Urban Environments*, initiated in 2021.

I would like to express my most sincere gratitude to my group of supervisors, Associate Professor Mario Plos, Adjunct Professor Morgan Johansson and Senior Lecturer Joosef Leppänen for their continuous support and guidance. Their expertise and engagement have been a constant source of inspiration to my work. Our frequent meetings are always teeming with valuable ideas and memorable moments. I look forward to continuing working alongside them in the upcoming years.

I would also like to thank our partners at KTH, Professor Anders Ansell, Adjunct Professor Mikael Hallgren, and doctoral student Viktor Peterson for the great collaboration in the research project. I would also like to extend my gratitude to all members of my reference group for their interest in my research and feedback. I also want to thank my colleagues and fellow students both at Chalmers and Norconsult for creating a good environment filled with interesting conversations and joyful moments.

I thank my parents and sisters who, despite the long distance, are always close to me and encourage me to continue moving forward.

Finally, Linnéa. You are the fuel that power my heart and soul. Your love and support have undoubtedly been the most valuable source of motivation. Thank you!

¡Gracias!

Fabio José Lozano Mendoza

Gothenburg, August 2023

List of publications

This thesis consists of an extended summary and the following appended publications:

I. Lozano F., Johansson M., Leppänen J., and Plos M.: *Blast strength of vapour cloud explosions in urban road environments: A numerical parametric study*. Submitted for publication. (2023).

II. Lozano F., Johansson M., Leppänen J., and Plos M.: *Probabilistic study of premature shear failure of slender reinforced concrete one-way slabs subjected to blast loading.* Submitted for publication. (2023).

These publications are hereafter referred to as **Paper I** and **Paper II**, according to the labelling in the list above.

AUTHOR'S CONTRIBUTION TO JOINTLY PUBLISHED PAPERS

The appended papers were prepared in collaboration with the co-authors. The contribution by the author of this licentiate thesis as well as the co-authors is described below.

In **Paper I**, the author conducted the literature survey, carried out the planning and execution of the numerical analyses and postprocessing of the results, and took major responsibility for the planning and writing of the paper. The co-authors assisted in the planning of the analyses, contributed to evaluating and discussing the results and participated in writing the paper.

In **Paper II**, the author participated in the planning of the work, conducted the literature study, carried out the analyses, contributed to the discussion of the results, and took the major responsibility for the writing of the article. The work builds on a gap in knowledge originally identified by Johansson. The co-authors assisted in the discussion of the results and writing of the paper.

OTHER PUBLICATIONS RELATED TO THE THESIS

In addition to the appended papers, the author of this thesis has also contributed to the following publications.

- Lozano F., Johansson M., Leppänen J., and Plos M. (2022): *Explosion loads in densified urban environments: challenges and needs*. XXIV NCR Symposium 2022, Stockholm.

- Peterson V., Lozano F., Johansson M., Hallgren M., Ansell A., and Magnusson J. (2023): *The effect of explosions in road tunnels on critical structural elements*. 48th ITA-AITES World Tunnel Congress, 2023, Aten.

Table of contents

1 Introduction

1.1 Background

The risk for explosion-related events in urban environments has increased in recent years in Sweden. It is enough to browse through news reports to get a glimpse of this worrying aspect of our society. Crimes associated with explosive materials have intensified since the 2010's. Between 2018 and 2022, an average of 190 incidents per year were reported [1]. The expected severity and/or frequency of such incidents may be much greater in countries exposed to greater societal threats. However, contrary to the impression one might get from news feeds, the risk for explosions in urban centres is not solely associated with intentional events. Indeed, explosions originating from accidental events may be as devastating. Moreover, the risk for accidental explosions is intrinsically connected to the functioning and continuous development of modern society, such as densification of existing urban environments.

Road transportation of flammable gases (such as liquified petroleum gas [LPG], liquified natural gas [LNG], biogas, and hydrogen) and explosive materials (such as ammunitions, fireworks, and dynamite) is an important potential source of accidental explosions in urban environments. In general, transportation of flammable gases occurs much more frequently than that of explosive materials. An accident during transportation of a flammable gas may result in the release or loss of containment of the gas, which could escalate into a vapour cloud explosion (VCE).

VCEs may result in considerable damage to people and infrastructure. In the near-field, besides large values of pressure, thermal effects such as radiation and fire constitute a hazard. Furthermore, the high pressure will push the surrounding air into motion as a blast wave, which may extend the damage zone to areas located at longer distances from the explosion source. Unfortunately, example of such events can be found in the press. In 2020, an accident involving a tanker loaded with around 25 tons of LPG (60% propane, 40% butane) occurred in Wending City, China. The tanker collided with a guardrail, which caused the tank to explode (cold BLEVE[1]). This was followed by a rapid release of gas into the atmosphere and the formation of a gas cloud, which ultimately gave rise to a VCE. This disaster resulted in 20 deaths and 175 injuries. Moreover, more than 200 buildings and several vehicles were damaged [3].

A relevant factor enhancing the risk for accidental explosions is the trend for densification of existing urban environments. Densification has been adopted by several municipalities in Sweden as a mean to provide their growing population with residential and office spaces [4], [5]. Densification may be achieved by permitting shorter distances between roads and nearby buildings. This means that the buildings will be closer to potential sources of VCEs on the road, which increases the severity of the load effects in the event of an explosion.

Another important factor is the rise of vehicles powered by alternative fuels (e.g., hydrogen, biogas) in combination with the supporting infrastructure (e.g., refuelling stations, pipelines). This entails an increase in the number of potential sources of unintended gas leakages and gas explosions in urban environments. The inhabitants of Stockholm, Sweden, were witness to an accident involving a bus fuelled by biogas (compressed natural gas [CNG]) that took place right outside *Klaratunneln* in 2019 [6]. The biogas container mounted on the roof of the bus collided with a metallic barrier, which caused rupture of the tank and subsequent dispersion of the gas. A gas cloud formed and was soon after ignited by the heat generated by the engine. This accident resulted in one person injured and damage in nearby buildings and vehicles.

[1] BLEVE stands for Boiling Liquid Expanding Vapour Explosion [2]

Altogether, the need to deal with explosion risks is becoming more commonplace within the urban development and construction industry. Eventually, design of reinforced concrete (RC) structures to withstand explosion loads may become a more common aspect of modern structural engineering. However, both the explosion phenomenon and the dynamic response of structures subjected to explosion loads are very complex in nature and properly handling it requires cross-disciplinary expertise and collaboration. According to Johansson et al. [5], there are three main areas that should be dealt with to properly evaluate and handle explosion loads in urban environments: risk analysis, explosion load, and structural response. If the conclusions from one of these subareas are based on incorrect assumptions, it is likely that the final solution will be negatively affected, either in the form of insufficient safety levels or as unnecessarily costly solutions.

Johansson et al. [5] showed several deficiencies within the construction industry in the three subareas in Sweden. In general, the wider structural engineering community lacks the specialized knowledge and tools required to design and assess structures that are subjected to explosion loads. Additionally, while risk analysts are experts analysing risk, they may lack the knowledge to understand the connection between a given accidental event, the resulting explosion load, and the response of the affected structures. Furthermore, structural engineers are used to working with statically loaded structures, while blast-loaded structures may respond very differently. This causes several problems within development projects, such as inadequate communication, lack of data and suboptimal designs.

The work presented in this thesis is part of a larger research project that seeks to tackle some of the needs identified by Johansson et al. [5], under the shared belief that a wider range of structural engineers and risk analysts should have the means to properly handle explosion loads in urban environments. Moreover, by gaining a good understanding of diverse complex phenomena, the project intends to develop simplified tools and methods that could be easily integrated with existing design approaches.

1.2 Aim and objectives

The overall aim of the PhD project is to expand the knowledge about explosion loads in urban environments and RC structures exposed to such extreme loading conditions. The latter is a continuation of a multidecade research program in this field at the Division of Structural Engineering at Chalmers, including [7]–[11]. However, investigation of explosion loads in urban environments, including the initiation and development of gas explosions and the propagation of the ensuing blast wave, is a new research avenue within Chalmers. The PhD project also draws from the experience gained at the Division for Concrete Structures at KTH, including [12], [13].

Based on the knowledge generated, the PhD project intends in the long-term to develop simplified approaches to deal with different aspects related to explosion threats in urban environments, both regarding the determination of the load from explosions and the response of RC structures exposed to these extreme loading conditions.

The work carried out in this stage of the PhD project was structured into two key research areas. Research Area I is concerned with the determination of the load from gas explosions on urban roads. Research Area II deals with the uncertainties associated with the failure mode of blast-loaded RC slabs.

The following specific research questions were defined for the individual research areas:

Research Area I:

- **RQ1**: *What is the expected strength of vapour cloud explosions on urban roads?*
- **RQ2:** *What are the most relevant parameters affecting the strength of vapour cloud explosions on urban roads?*

Research Area II:

- **RQ3:** *What is the likelihood of brittle shear failure in blast-loaded slender RC one-way slabs considering the uncertainties related to the material properties, geometry, and resistance models?*
- **RQ4:** *How can the confidence level regarding ductile failure of blast-loaded slender RC one-way slabs be increased?*

1.3 Methodology and scientific approach

With the purpose of meeting the specific research questions, the research work in this thesis was structured as presented in Figure 1.1.

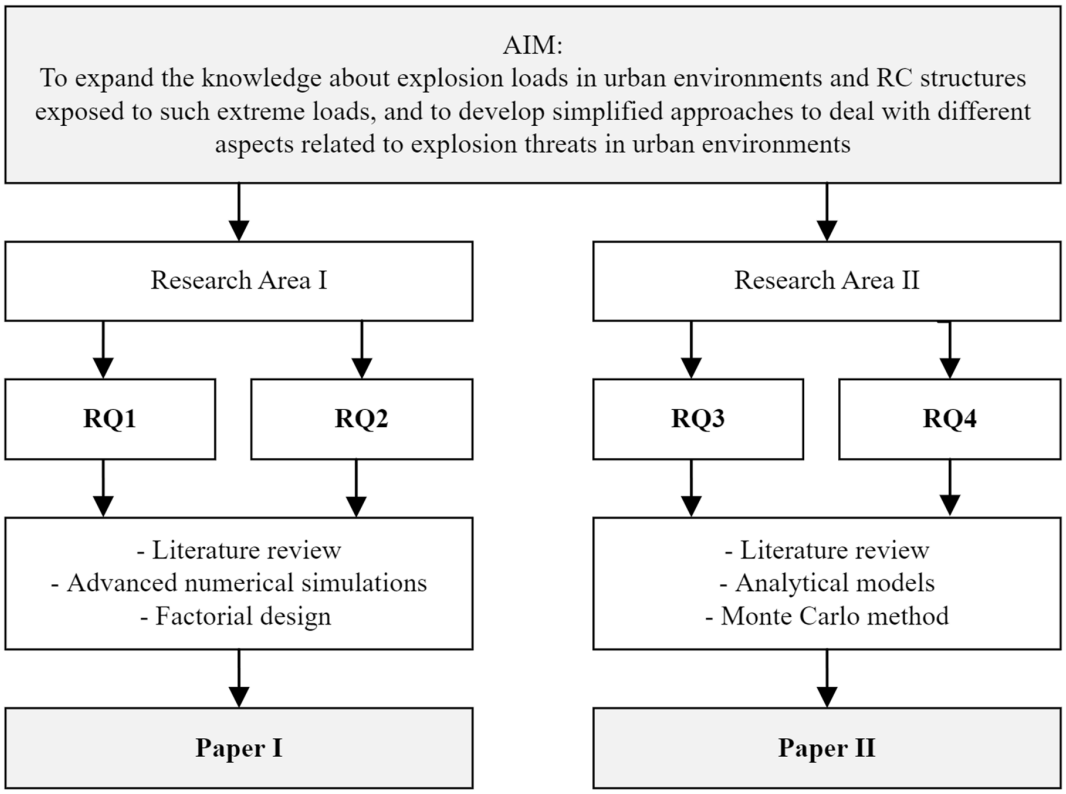

Figure 1.1. Connection between the overall aim of the research project, research questions for this part of the PhD project, and the work conducted.

As Figure 1.1 shows, the methodology chosen to carry out the research was a combination of literature review with advanced numerical calculations and more simplified analytical methods. The numerical models were intended as an approximative representation of a complex

phenomenon. The motivation behind this choice was that numerical modelling has a relatively low cost in comparison with experimental campaigns. Moreover, numerical modelling enables the investigation of multiple scenarios and thus a more extensive parametric study. In addition, sampling of results from numerical models can be carried out over a larger area compared with what can be achieved with experiments. However, where relevant, the numerical models were validated against experimental data available in the literature.

To conduct the work concerning Research Area I, numerical simulations based on *Computational Fluid Dynamics* (CFD) were performed. The work was supported by preliminary sensitivity studies, including grid sensitivity analysis and comparison against experiments for the choice of cell grid size. The setup and geometry of the studied cases were designed with the intention to allow for potential future experimental studies. The principles of *factorial design* were implemented to carry out a parametric study in two stages. Factorial design is a structured method which enables investigation of the effects of several factors on a response variable with a limited number of simulations, which can balance the high computational requirements of the CFD calculations. Much of the work carried out in Research Area I is compiled and presented in **Paper I**.

The work performed within Research Area II deals with uncertainties involved with the failure mode of blast-loaded RC one-way slabs. The strategy chosen to evaluate the effects of these uncertainties was to use simplified analytical models for determination of the resistance of RC slabs in combination with the conventional *Monte Carlo* method. The use of simplified analytical models facilitated a large number of iterations with the Monte Carlo method. Additionally, an iterative process with the Monte Carlo method was used to find partial factors to improve the confidence level regarding the preferred failure mode during the design of the RC slabs. This work is presented in **Paper II**.

A more detailed description of the methodology followed is presented for each research area under their respective chapters.

1.4 Limitations

A summary of the main limitations of the presented work, including the appended papers, is described in the following:

Research Area I:

- Due to the high computational demands to run the CFD simulations of gas explosions, only one type of gas was considered. Furthermore, some important parameters such as the geometry and ground clearance of the vehicles were kept constant during the calculations.
- The study carried out in this thesis considered only explosions scenarios in open areas. Explosions in confined environments such as tunnels or street overbuilds are outside the scope of this thesis.
- The only source of congestion within the gas cloud that was considered in the CFD calculations was vehicles on the road. Other potential obstacles such as noise barriers or nearby structures were not included.

Research Area II:

- The RC slabs studied here had a relatively low complexity. Thus, they are more representative of single elements rather than of complete structural systems.
- To determine the design shear force in the blast-loaded RC slabs, the concept of *equivalent static load* was used. This simplified method was adopted as it enabled the analysis of thousands of different cases with a limited amount of resources. However, the real distribution of shear in a blast-loaded element may be different, particularly for highly impulsive loads.

1.5 Original features

The original features of the present work are summarized as follows:

Research Area I:

- Even though there exist several guidelines for estimation of the strength of gas explosions in the literature, most of these are calibrated for conditions in the petrochemical industry. No clear explicit guidelines or methods for the estimation of the strength of gas explosions on urban roads are available in the literature. This work directly addresses this knowledge gap with the help of advanced numerical simulations.

Research Area II:

- This work raises awareness about the risk of premature shear failure in structures designed to fail under bending failure due to uncertainties involved in the design of the structure. Furthermore, the study proposes a method to decrease the likelihood of brittle shear failure.

1.6 Outline of the thesis

This thesis consists of an extended summary and two appended papers submitted for publication in reviewed scientific journals. The introductory chapters provide background knowledge and complementary material relevant to the work presented in the appended papers.

Chapter 1 gives the background, aim and research questions of the thesis. Moreover, the scope, limitations, a general description of the research methodology and original features are presented.

Chapter 2 introduces the fundamental knowledge of explosions, blast loading and structural response. This knowledge constitutes the theoretical background relevant for this study.

Chapter 3 presents the methodology and results of the research work concerning gas explosions on urban roads. This topic is further explored in **Paper I**.

Chapter 4 presents the methodology and results of the research work regarding uncertainties and design of blast-loaded RC one-way slabs. This work is the focus of **Paper II.**

Chapter 5 contains the main conclusion drawn from this study and suggestions for future research.

2 Theoretical background

2.1 Overview

Structures located nearby roads on which transportation of flammable gases is permitted are exposed to a risk for powerful accidental vapour cloud explosions[2] (VCE). An accident on the road involving a vehicle hauling flammable gas may result in the unintentional release of the gas. Given the right circumstances, the gas may spread and form a combustible fuel-air cloud that may explode violently. The risk for such an event has increased in recent years due to diverse factors such as densification of urban environments and adoption of alternative fuels (e.g., hydrogen, biogas) to power urban vehicles. Densification entails a reduced distance between the structures and potential sources of accidental explosions on the roads, which results in the increase of the severity of the effects in the structures should an explosion occur. Moreover, a greater number of vehicles running on alternative fuels means an increase in the number of potential sources of gas explosions.

In an engineering context, risk is often defined as the product of the frequency and consequence of an event, as given by Eq. (2.1).

$$\text{Risk} = \text{Frequency} \times \text{Consequence} \tag{2.1}$$

From the lens of this definition, it is evident that the risk for accidental VCEs in urban environments has been enhanced on both of its components. This means that when accounting for gas explosion hazards in urban development projects, it may not be sufficient to mitigate the risk by focusing on reducing the frequency of accidental releases. This could be achieved by, for instance, strict requirements on vehicle safety, training of personnel, or restrictions on routes. Instead, it may also be necessary to design nearby structures to withstand blast loads resulting from gas explosions on the road as a last barrier to protect people and assets.

Consideration of blast loading during the design of reinforced concrete (RC) structures is today usually reserved for a selected group of high-risk and essential structures. Furthermore, this type of design requirement is normally outside the purview of the general engineering community. However, an increase of the risk for gas explosions on urban roads may eventually lead to stricter design requirements even for low-profile RC structures that are traditionally not designed for this type of action. That is, blast-resistant design of RC structures may become a more common aspect of modern structural engineering.

For an optimal design of a RC structure against blast loading, good knowledge of explosions, blast loads, and dynamic response of structures is necessary. Moreover, appropriate calculation and design methods are required. In the conceptual phase of the design process, it is beneficial to have access to fast engineering methods that allow for quick evaluation of multiple scenarios. In the detailed engineering phase, more advanced methods for the final calculation of loads from explosions and the response of the structure may be required. But even in the detailed engineering phase, simplified but sufficiently accurate methods could be useful, both for checking the plausibility of the results produced by advanced methods, but also for carrying out the final design, depending on the complexity of the case.

[2] The term *gas explosion* is used interchangeably in this document to refer to vapour cloud explosions.

2.2 Consequence analysis of gas explosion risk

A quantitative risk analysis is usually performed to evaluate the consequences of accidental releases of flammable gases on the road. An essential step within this process is the identification of the hazards and definition of potential accident scenarios. For the identified scenarios, the expected frequency and consequences are then determined.

Figure 2.1 gives a typical event tree outlining different outcomes following an unintended release of flammable gas into the atmosphere. Information about such outcomes can be found in e.g., [14], [15]. The figure also shows the likelihood of the different events according to [16]. Evidently, a gas explosion is not the only potential result of a release of flammable gas. Indeed, if there is no suitable ignition source, or if the concentration of the fuel-air mixture is outside the flammability limits, combustion may not initiate. For such a case, the gas may dilute without noticeable consequences. However, if ignition happens immediately, before the fuel blends with the surrounding air, a *jet fire* will occur. Furthermore, if the vessel is damaged or weakened by the accident or jet fire, a *BLEVE* (Boiling Liquid Expanding Vapour Explosion) may follow. Finally, if ignition is delayed, the gas may have sufficient time to spread and form a premixed cloud of flammable gas and air. This cloud can engulf nearby vehicles or other objects on or near the road. If this cloud is ignited, combustion may develop as a *flash fire* or a *gas explosion*. The distinction between these two outcomes lies in the overpressure generated. A flash fires is a weak combustion producing low pressure whose main hazard is heat radiation. Conversely, a gas explosion is the combustion of a premixed cloud which causes rapid and significant increase of pressure. However, there are no hard criteria to separate the two outcomes. According to [17], combustion of a premixed cloud leads to flash fires 60% of the time, while the remaining 40% corresponds to gas explosions. However, the resulting overpressure depends strongly on the conditions of the surroundings. For that reason, some authors do not separate the two outcomes, but instead rate the resulting explosion in terms of its strength. In this thesis, the last approach is followed.

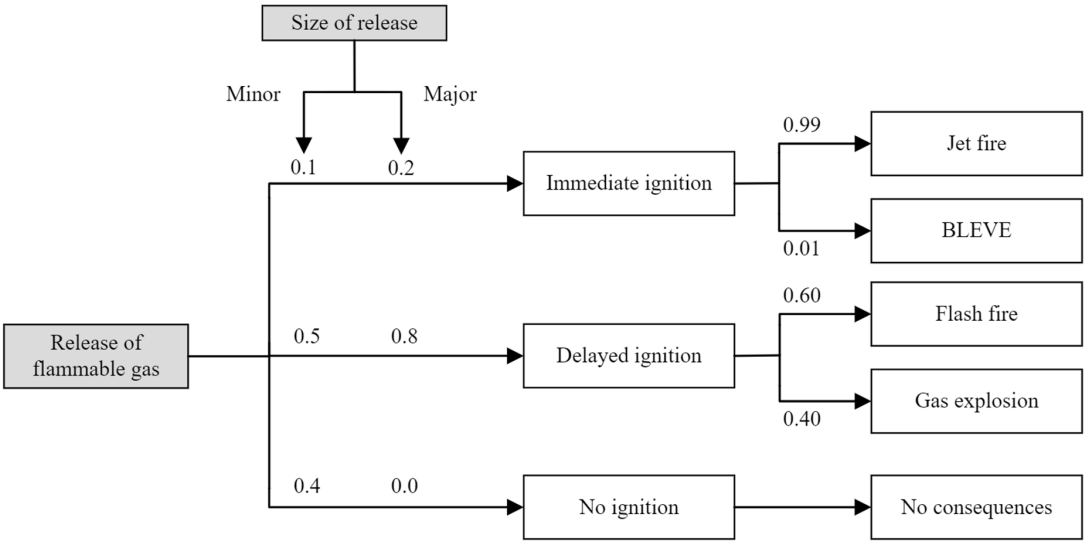

Figure 2.1. Event tree outlining different outcomes following a release of a flammable gas on a road. The numbers represent the likelihood of the outcomes according to [16].

In Sweden, risk analyses often indicate that delayed ignition is the most likely outcome [18], [19]. However, the product of such risk analyses is usually in terms of the estimated number of fatalities and often no specific loads for the design of the affected structures are provided. Results concerning the societal risk associated with the accidental events are usually presented as F-N curves, in which F is the cumulative frequency of accidents that produce N or more fatalities. To judge if the calculated risk is acceptable, the computed F-N curves are compared to limiting curves that divide the region into three areas: acceptable risk, ALARP (as low as reasonable possible), and unacceptable risk. An example of this comparison is illustrated in Figure 2.2.

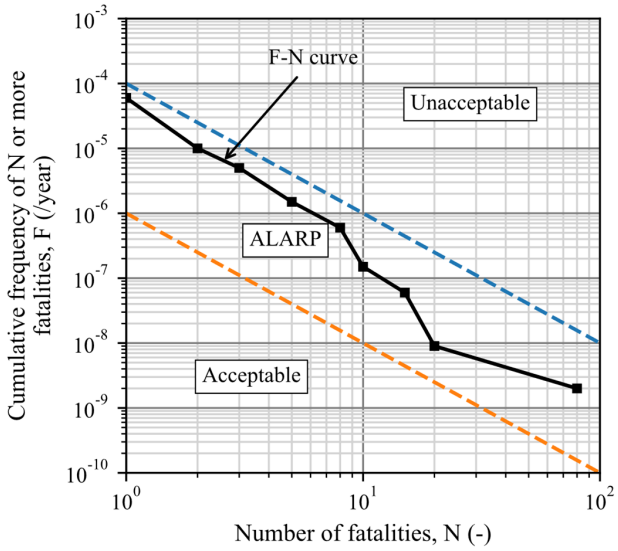

Figure 2.2. Example of comparison of a F-N curve against risk acceptability criteria. Adapted from [20].

Detailed engineering involves the estimation of the explosion load and response of the structure. This is a complex process that requires cross-disciplinary expertise. Figure 2.3 shows a schematic representation of different aspects that should be considered during this process. The first step is identification of the hazard, which also includes characterization of the source (e.g., type of gas, rate and duration of leakage), followed by the description of the dispersion scenarios (e.g., size of premixed gas cloud, concentration of the cloud). Thereafter, different explosion scenarios should be investigated, including different assumptions regarding location and energy of the ignition source and description of the combustion of the cloud. The explosion will generate a blast wave that will propagate throughout the environment, eventually loading the studied structure. The description of the blast load acting on the structure may become highly complex due to the intricate nature of urban environments. Finally, the dynamic response and resistance of the blast-loaded structure should be investigated. The process presented in Figure 2.3 is complicated and different challenges and opportunities exist in each step. It should also be noted that the scope of the work in this thesis falls within two specific steps in this process: explosion scenarios and structural response.

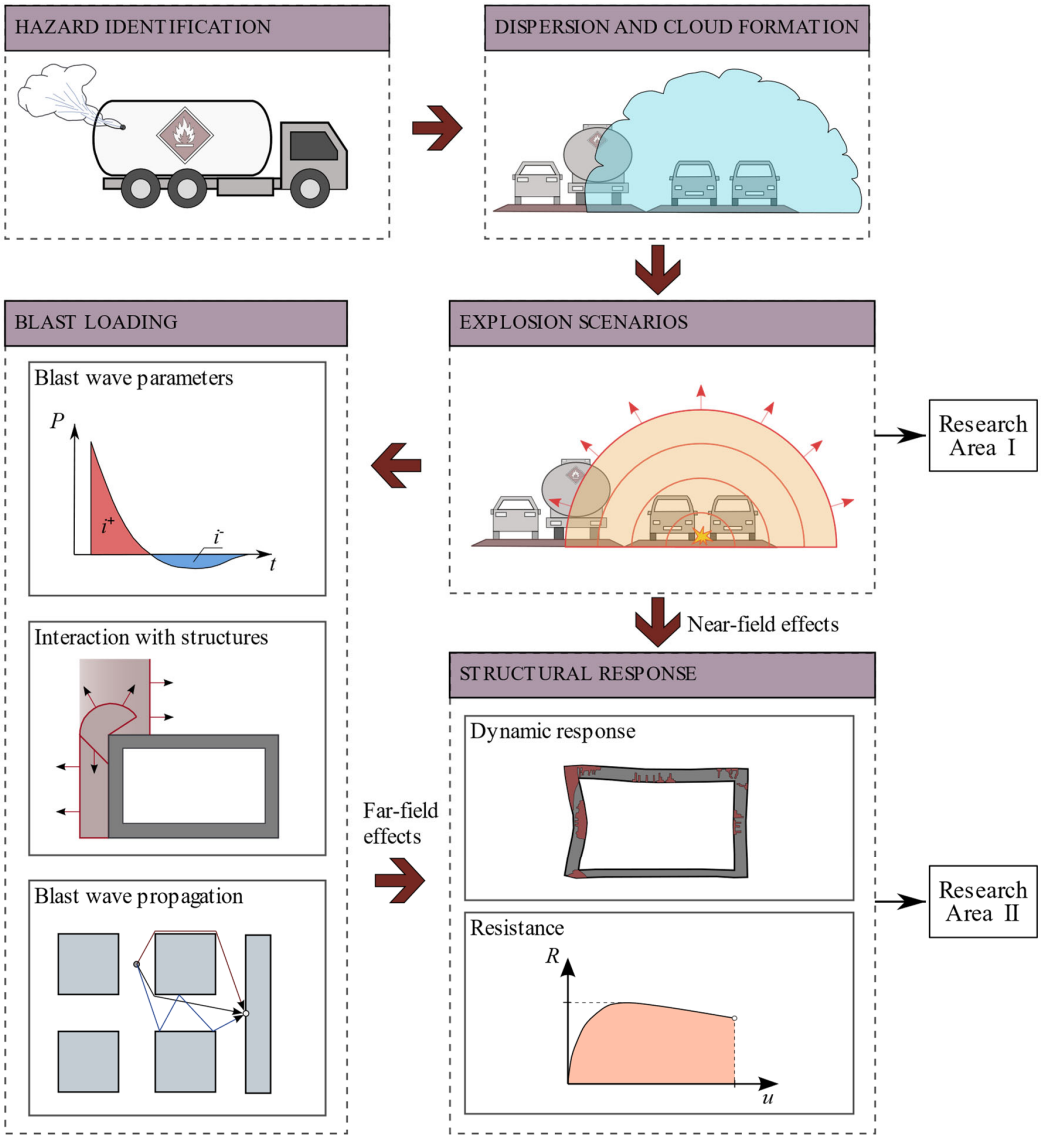

Figure 2.3. Schematic representation of different aspects that need to be considered when dealing with gas explosion threats in urban environments.

2.3 Explosions

2.3.1 Deflagration and detonation

In general terms, an explosion can be defined as a release of energy over a very short time. The source of this energy could be chemical (such as explosive charges or fuel-air mixtures) or physical (such as a rupture of a vessel containing a pressurized liquid)[3] [21]. This energy is dissipated by different mechanisms, such as blast waves or propulsion of projectiles.

An explosion of a fuel-air mixture is usually termed vapour cloud explosion (VCE). The flame front (i.e., interface between burned and unburned material) in VCEs can progress in two

[3] Nuclear explosions are outside the scope of the research project.

different modes, namely: deflagration and detonation. In a deflagration, the flame front is propagated by conduction and molecular diffusion of heat [15]. Laminar flames in a deflagration are characterised by a reaction zone (where heat is generated by chemical reaction) and a preheating zone (where the unburned material is heated and preconditioned for ignition), see Figure 2.4. In deflagrations, the flame front always travels at subsonic speeds relative to the unburned gas ahead of the flame, as molecular diffusion is relatively slow. However, relative to a stationary observer, the flame speed may increase up to 500 – 1000 m/s [14]. The vast majority of accidental VCEs reported in the literature were deflagrations. Thus, unless specified otherwise, the term VCE refers to deflagration in this work.

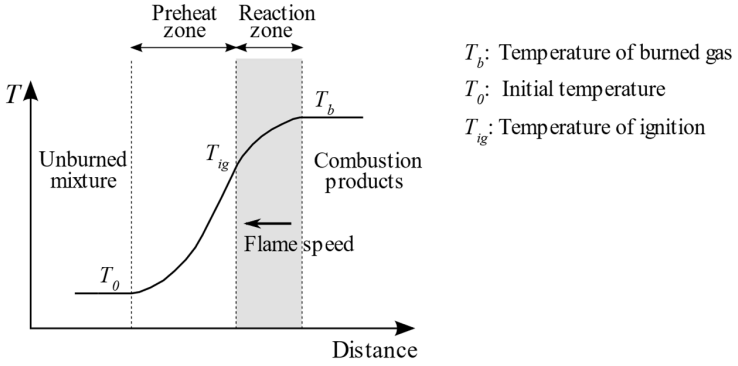

Figure 2.4. Structure of a laminar flame. Adapted from [22].

In a detonation, the reaction front is propagated as a strong shock wave, which compresses the unburned material past its autoignition temperature. Detonation velocities are always greater than the speed of sound. Fuel-air mixtures initially at ambient pressure can reach detonation velocities of up to 2100 m/s [15]. Detonation of a gas cloud can initiate either directly due to high-energy ignition or as *deflagration-to-detonation transition* (DDT), a process in which a deflagration evolves into a detonation. Detonation of gas clouds is an uncommon event in society and examples of such detonations are normally from research experiments. However, a few cases of accidental detonations of gas clouds have been reported [23], [24]. This means that the risk for detonation cannot be ruled out without a careful evaluation of the scenario.

A detonation is the most violent form of combustion of a gas cloud and can cause the most severe damage due to the large overpressure generated by the supersonic shock front. The maximum pressures produced are in the order of 1800 to 2000 kPa [15]. On the other hand, the generated overpressure in deflagrations depends on the burning rate. Low flame speeds usually result in minor overpressure (i.e., flash fires), while higher flame speeds generate greater overpressure. The evolution of a deflagration is a complex process because flame speed and pressure build-up are not unique for a given fuel-air mixture. Instead, the resulting explosion strength varies over a wide range depending on many factors such as degree of confinement and congestion, turbulence, venting, location of ignition, and environmental conditions.

2.3.2 Effect of confinement and obstruction in deflagrations

The resulting flame speed and explosion pressure in a VCE depend strongly on the geometrical conditions of the environment where deflagration occurs. This includes both the geometry and arrangement of obstacles within the cloud and the geometries enclosing all or part of the cloud.

When the flame propagates through the gas cloud, there are two main mechanisms leading to pressure increase: fast burning rate and flame propagation in a confined space [14]. In most accidental explosions, the combination of these two effects causes the pressure build-up. In general, an increased flame speed enables higher explosion pressure. If the gas cloud is ignited with a weak ignition source (e.g., a spark), the flame starts propagating at a laminar speed. The basic mechanism of propagation of the laminar flame front is molecular diffusion of heat and mass (see Figure 2.4). As the flame consumes the unburned material, the combustion products will expand up to 8 or 9 time the original volume. Because of this expansion, the unburned gas will flow ahead of the flame. Interaction of this flow with surfaces (e.g., ground and ceiling) and objects within the cloud will create velocity gradients that will stretch the flame front. This expands the original surface area of the flame, which in turn results in enhancement of the flame speed. When the flame speeds are sufficiently high, turbulent conditions may form ahead of the flame, both due to the velocity gradients breaking down into turbulent shear layers and turbulent vortices generated in the wake of obstacles [25]. When the flame enters the turbulent region, it will be stretched and wrinkled further, which boosts the burning rate. Furthermore, for high-intensity turbulence, the small-scale vortices will enhance the transport of heat and mass across the flame front, which accelerates the flame further. The increased burning velocity will cause the explosion pressure to rise.

If there is only one single row of obstacles in the path of the flame, the flow field will subside after passage of the flame front, and the flame front speed will decay. However, if multiple layers of obstacles are present, the increased flame speed will enhance turbulence generation ahead of the flame around the subsequent layer of objects. This mechanism of flame acceleration due to repeated obstacles constitutes a strong positive feedback loop. This loop is shown in Figure 2.5.

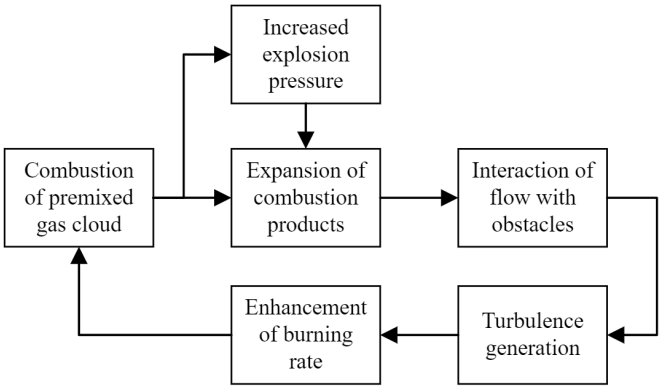

Figure 2.5. Positive feedback loop for flame acceleration due to repeated obstacles [14].

The main effect of confinement is preventing the expansion of the flow in one or more directions. A deflagration propagating in a tube normally requires lower flame speed to produce the same explosion pressure than a flame propagating in unconfined conditions. Furthermore, the interaction of the flow with confining surfaces also generates turbulence.

To characterize confinement and obstruction, it is common to use parameters such as volume blockage ratio (VBR), obstacle diameter, and pitch (spacing) between rows of obstacles. Research shows that increasing VBR will result in higher pressure [26], [27]. Furthermore, for the same VBR, smaller obstacle diameters will likely increase the explosion pressure. The

reason for this is that smaller obstacles deployed over a greater number of repeated layers will allow the positive feedback loop in Figure 2.5 to cycle more times.

Other aspects such as the shape and arrangement of the objects may also have a significant effect on the explosion pressure [14]. Square obstacles normally lead to higher pressure than cylindrical objects for the same VBR. The main reason for this is that the turbulence in the wake of obstacles with sharp corners is more intense than that produced by round obstacles. Regarding arrangement of the obstacles, staggered configurations may produce greater explosion pressure than structured arrangements.

2.3.3 Predictive models for gas explosions

Experimental investigation would be the ideal strategy for estimating the possible consequences of gas explosions. However, carrying out gas explosion experiments, particularly at large scales, is usually prohibitively expensive. Therefore, different models have been developed for predicting the consequences of gas explosion scenarios. In the literature, three categories are normally distinguished: empirical models, phenomenological models, and numerical models [28]–[30].

Empirical models consist of correlations or general guidelines developed from analysis of experimental results. These are simplified methods that allow for fast and (normally) conservative approximations of the blast loading caused by the gas explosion. Some of these methods are introduced in Section 2.4.2. However, the methods have several limitations, such as difficulty to represent complicated geometries and difficulty to choose the blast strength representing the explosion source. Unlike empirical models, phenomenological models attempt to describe the governing physical processes in an explosion based on simplified description of the geometry and correlations derived from a combination of experimental data and theoretical models. The SCOPE model [31] and the CLICHE model [28] are examples of this type.

Numerical models are based on the fundamental partial differential equations governing fluid flow and the combustion process, which are numerically solved with the principles of computational fluid dynamics (CFD). These include the basic equations for conservation of mass, momentum and energy (Navier-Stokes equations) in addition to physical models to describe turbulence and combustion [32]. CFD codes are normally classified into “simple” and “advanced” models. Simple CFD codes, such as EXSIM [32], FLACS-CFD [33], and PDRFoam [34], rely on the Porosity Distributed Approach (PDR) [35] to greatly simplify the geometrical conditions by representing sub-grid elements (i.e., objects smaller than the grid cell size) as volume and area porosity and resistance factors. This approach allows for coarser grids, which enables simulations of large-scale cases. In contrast, more advanced codes attempt to describe the geometry as reliably as possible. High computing power requirements, long run times, specialized knowledge by the user, and high costs are the main limitations commonly associated with numerical models.

2.4 Blast loading

2.4.1 Free-field blast waves

In an explosion of a fuel-air mixture, the combustion products expand to a volume much larger than the original volume. This means that the chemical energy in the fuel-air mixture is partially converted into mechanical energy. The mechanical energy is transmitted into the neighbouring atmosphere in the form of a blast wave, whereby the surrounding air is pushed outwards from

the explosion centre [21]. Besides blast wave generation, the mechanical energy can also be dissipated through other processes, such as projectile ejection.

At a particular fixed point, the blast wave caused by VCEs is experienced as a transient change in state parameters such as pressure, density, and temperature [15]. In the context of blast-resistant design, it is common to characterize the blast wave based on its pressure-time history. The shape of the blast wave depends on the amount of energy released, the speed of release, and the distance from the explosion centre. According to [36], three blast wave regimes in free-field conditions can be distinguished, namely: shock wave, pressure wave, and acoustic wave. A schematic representation of the pressure-time history for each regime appears in Figure 2.6. A positive and negative phase can be distinguished for all cases. A shock wave is a fully developed compression wave, characterized by an immediate and drastic increase of pressure, followed by a rarefaction wave. The shock wave may be treated as a discontinuity for most practical purposes. The shock wave propagates at supersonic velocity relative to the gas immediately ahead of the shock, i.e., the gas ahead is undisturbed by the shock. Shock waves are typical for strong explosions, such as detonations or strong deflagrations. Weak explosions, on the other hand, give rise to acoustic compression waves, characterized by a gradual increase of pressure, followed by a rarefaction wave. Pressure values for this type of blast wave are relatively low. Explosions of intermediate strength usually generate pressure waves, for which a noticeable increase of positive pressure is achieved in a relatively short time. However, the rise time is not zero for this type of wave. At a longer distance from the explosion centre, most blast waves tend to steepen up to shock waves. Note that some authors group pressure waves and acoustic waves into one single category, e.g., [37].

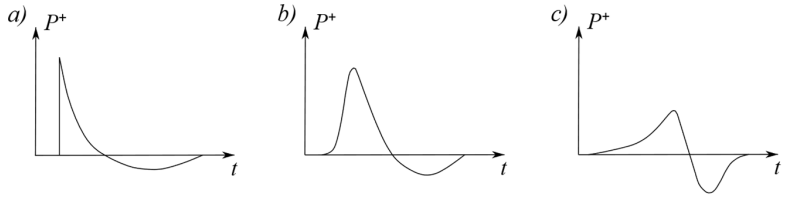

Figure 2.6. Schematic representation of the different blast shapes according to [36]: a) shock wave; b) pressure wave; c) acoustic wave. The figures are not drawn on the same scale.

Blast waves are usually defined with the help of the so-called blast wave parameters. The different blast waves parameters are described in Figure 2.7. The parameter ΔP represents the overpressure and can be determined with Eq. (2.2), in which P is the absolute pressure and P_0 is the ambient pressure (approx. 100 kPa). The parameter ΔP^+ represents the peak overpressure. The use of overpressure is preferred in the literature because any damage in the structures will be caused by the pressure relative to the ambient pressure.

$$\Delta P = P - P_0 \tag{2.2}$$

As the blast wave propagates unimpeded by the environment, the explosion energy is distributed over an increasingly larger volume. This results in a decrease in the peak overpressure and the specific impulse of the blast wave as the distance from the explosion centre increases. This process is called free-field pressure decay.

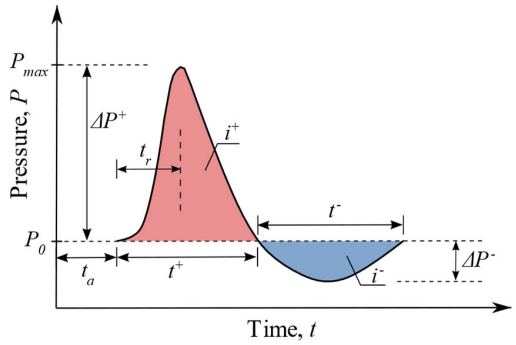

ΔP^+: Peak overpressure
ΔP^-: Peak underpressure
i^+: Positive specific impulse
i^-: Negative specific impulse
t^+: Duration of positive phase
t^-: Duration of negative phase
t_a: Time of arrival
t_r: Rise time

Figure 2.7. Definition of blast wave parameters.

2.4.2 Estimation of blast loading from VCEs

Different empirical methods to estimate the parameters of the free-field blast load from VCEs can be found in the literature. Examples of such methods include the TNO Multi-Energy method (TNO-MEM) [38], the Baker-Strehlow-Tang (BST) method [39], [40], and the Congestion Assessment Method [41].

The TNO-MEM is one of the most used methods because of its simple and coherent conceptual framework. According to this method, only those regions within a gas cloud that are partially congested or confined can produce a strong blast. These regions are commonly called *blast sources*. Several blast sources can exist within a large gas cloud. In contrast, the remaining unconfined or uncongested gas volume will not contribute significantly to overpressure generation. For the determination of the blast wave parameters, the TNO-MEM provides blast charts for side-on static overpressure, dynamic overpressure, and positive phase duration as a function of the energy-scaled distance. Each chart consists of a set of 10 curves for different strength classes, see Figure 2.8. The energy-scaled distance depends on the estimated energy of the blast source, which the TNO-MEM relates to the volume of gas in the blast source. The most challenging aspect of the TNO-MEM is possibly the estimation of the blast strength. Note that the terms *blast strength*, *explosion strength*, *charge strength* and *source strength* are commonly used interchangeably in the literature to refer to the overpressure generated by the gas explosion at the source of blast. In this sense, greater strength means that the generated blast wave will exhibit greater peak overpressure. Guidelines for determining this parameter within the context of the TNO-MEM can be found in the literature, e.g., [30], [42]–[44].

a) Overpressure chart

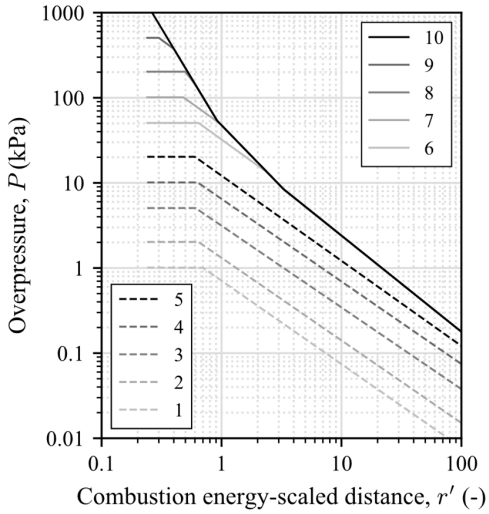

b) Positive phase duration chart

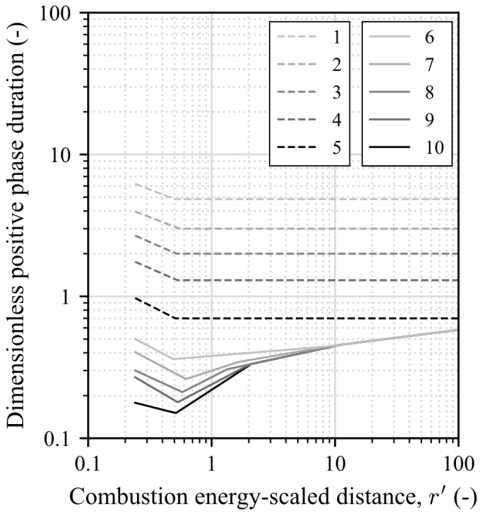

Figure 2.8. Charts for side-on overpressure and positive phase duration as a function of energy-scaled distance and strength class (1-10) according to the TNO-MEM. Adapted from [38].

2.4.3 Interaction of blast waves with structures

When the shock front impinges on a surface, the pressure is enhanced by the abrupt stop of the movement of the particles. This phenomenon is called *reflection* [45]. The reflected particles have a velocity equal in magnitude to the original velocity but with opposite direction, which produces the effect of a reflected shock front travelling back through a medium with a higher pressure than the surrounding atmosphere. The reflected pressure depends on the incident (side-on) pressure and the incident angle.

Because of *diffraction*, the blast load acting on a structure varies on different sides of the structure. This process is illustrated in Figure 2.9. The greatest value of pressure is registered on the front face, where the pressure rises to the reflected value. The load experienced by the top and side faces corresponds to the side-on pressure, as no reflection occurs on surfaces parallel to the direction of propagation. When the blast wave has traversed the length of the building, the rear face is loaded with a pressure close to the side-on overpressure. However, depending on the length of the building, the side-on overpressure behind the structure may be noticeable lower than the side-on overpressure at the front of the structure due to free-field decay.

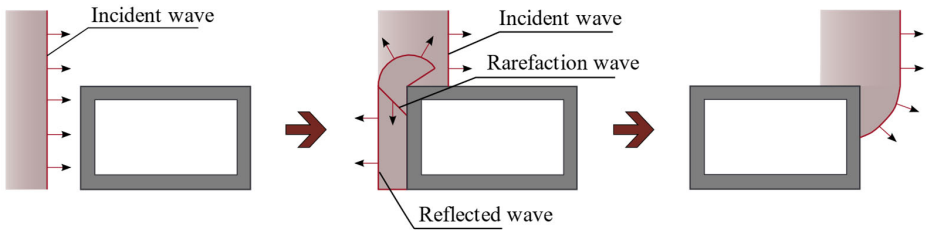

Figure 2.9. Representation of the interaction of the blast load with a finite-size structure.

It should be noted that the pressure difference between the front face and the side and top faces gives rise to a rarefaction wave that travels inwards through the front face from the edges, effectively decreasing the pressure in the front face down to the stagnation pressure (i.e., the combined effect of the side-on overpressure and the dynamic pressure[4]) [46]. The influence of this process, called *clearing*, depends on the size of the structure. The typical pressure profile for finite-size front faces is shown in Figure 2.10. In infinitely large structures, clearing is negligeable. Conversely, in infinitely small structures, clearing occurs immediately. This means that in infinitely small structures the pressure on the "front face" corresponds to the side-on overpressure.

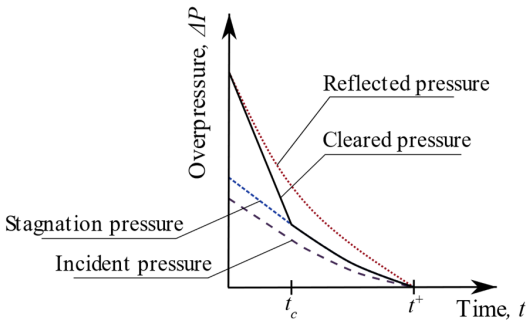

Figure 2.10. Blast load on the front face of a finite-size structure. Adapted from [46]

2.4.4 Propagation of blast waves in urban environments

The evolution and propagation of blast waves in urban environments differ substantially from those of free-field blast waves [47]–[49]. The interaction of the blast wave with obstacles along its path gives rise to physical phenomena such as reflection, diffraction and superposition which significantly increase the complexity of the loading. In the literature, the effects of such phenomena are usually grouped into two concepts: channelling and shielding. *Channelling* refers to the enhancing effect of confinement due to nearby structures and coalescence of multiple waves that have reflected from or diffracted around buildings. *Shielding*, on the other hand, accounts for the attenuating effect from objects located between the studied building and the explosion centre. Figure 2.11 shows conditions propitious for channelling and shielding.

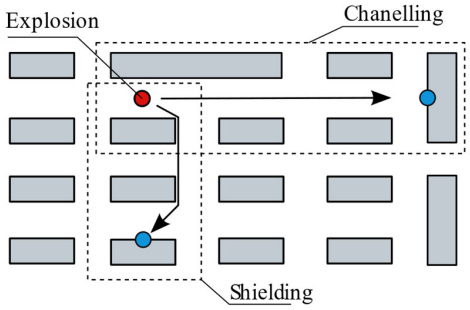

Figure 2.11. Channelling and shielding in urban environments.

[4] The dynamic pressure is the *increase* in pressure that a moving fluid would experience if brought to rest [45].

2.5 Structural response

2.5.1 Overview

Blast waves acting on RC structures impose large external energy on the structures over a significantly short time. When subjected to such conditions, both the response of the structure and the material properties may be considerably different than those of statically loaded structures [50], [51]. Due to the dynamic loading, the structure will experience acceleration which entails that inertial effects (related to the mass of the structure) will influence the response.

Furthermore, dissipation of the imposed energy by means of large inelastic deformation gains an important role for blast-loaded structures [52]. The blast wave produces an external work, W_e, which needs to be balanced by an internal work, W_i, in the structure. Figure 2.12 gives a schematic representation of the load function *F(u)* and the resistance function *R(u)* as a function of the deformation, u, of a blast-loaded structure. The external work W_e caused by the load is given by the area under *F(u)*. Likewise, the area under *R(u)* from origin to a certain deformation u_{tot} represents the internal work W_i required to counteract W_e. Evidently, the total internal work that can be mobilized before failure depends both on the deformation capacity, u_d, and the load resistance, R_d, of the structure. However, it is often more practical and economical to design the structure to dissipate the energy imparted by means of a large inelastic deformation, rather than relying on a large load resistance. Therefore, it is necessary to ensure that blast-loaded structures have sufficient plastic deformation capacity to develop the required internal work.

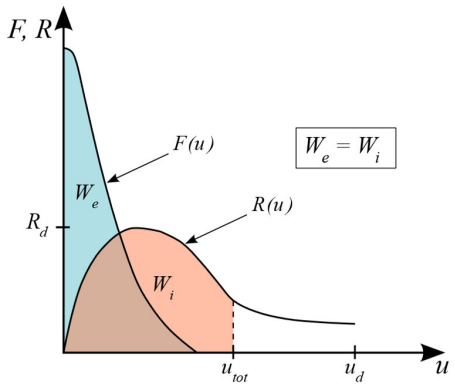

Figure 2.12. Schematic illustration of the external work W_e imposed by an external blast load F(u) and the corresponding balancing internal work W_i due to the internal resistance R(u). Adapted from [52].

The characteristics of the blast loading (i.e., peak overpressure, rise time to peak overpressure and the duration of the loading) will influence the response of the structure [53]. When studying blast-loaded structures, it is common to relate the duration of the load, t_d, to the natural period, T, of the structure under consideration. Cormie et al. [54] distinguishes between three different regimes based on the ratio t_d/T, as shown in Table 2.1. The behaviour of the structure changes for each regime. Under quasi-static loads, the duration of the load is longer than the period. For this case, the structure reaches the maximum displacement before the blast load undergoes any significant decay. Here, the maximum displacement can be described as a function of only the peak load and the stiffness of the structure. Under impulsive loading, the load fully decays before the structure has time to respond significantly. Thus, maximum deformation is achieved

at a time greater than t_d. For this type of loading, the response is in principle a function of the impulse, stiffness, and mass. That is, the actual peak load is not relevant. The response under dynamic loading is the most complex, as pressure decay and the response of the structure are intrinsically connected. This type of loading often requires complete solution of the equation of motion.

Table 2.1. Blast loading regimes according to [54].

Regime	Criteria
Impulsive	$t_d/T < 0.1$
Dynamic	$0.1 < t_d/T < 10$
Quasi-static	$10 < t_d/T$

2.5.2 Dynamic material properties

RC structures subjected to extreme transient loadings (such as blast waves or impact) may develop strain rates in the material that are substantially higher than those under static loading. For such cases, the mechanical properties of both plain concrete and reinforcing steel may be notably affected by the high strain rates. This manifests as enhancement of the mechanical properties of the materials (e.g., strength and Young's modulus) compared to the corresponding properties in statically loaded structures. This phenomenon is commonly known as *strain rate effects* [55], [56]. The enhancement is usually described by a *Dynamic Increase Factor* (DIF), which is the ratio between the dynamic and the static value of the material property. In concrete, this effect is particularly significant for tensile strength, for which the dynamic strength can be up to seven times larger than the static tensile strength. The strain rate effect is less significant for other properties but the DIF value may still be more than two for compressive strength and up to about 1.6 for the Young's modulus [8]. In reinforcing steel, the strain rate effects influence both the yield strength and the ultimate strength. However, the Young's modulus remains unchanged [8]. The DIF values are provided by different design guidelines and regulations. Johansson and Rempling [57] compiled DIF values from different standards. It is worth mentioning that a DIF of 1.0 is assumed in both Eurocode 2 [58] and the design regulations by the Swedish Fortification Agency [59].

2.5.3 Failure modes of blast-loaded RC elements

In this thesis, the discussion regarding failure of blast-loaded RC structures is limited to simply supported beams. Simply supported RC beams subjected to a uniformly distributed load typically exhibit two types of failure modes: *bending failure* and *flexural shear failure*, see Figure 2.13. A RC beam failing under bending usually exhibits a ductile response with large plastic deformations. Such element develops nearly vertical cracks in the mid-region that propagate deep into the section. Failure occurs either due to crushing of concrete in the compression zone or due to yielding and subsequent fracture of the reinforcement [60]. However, if the supports provide the required anchoring, the load-carrying capacity of the element may be significantly enhanced by membrane action. Conversely, flexural shear failure is typically characterized by brittle behaviour with limited deformation capacity. The prominent feature of the flexural shear mechanism is the occurrence of a principal diagonal crack that extends to the compressive fibre at the top of the section [61]. The principal crack evolves from a flexural shear crack, which means that some form of flexural behaviour is required to develop this type of failure. For this reason, some authors couple the bending and flexural shear

behaviour during the design of the elements by reducing the bending capacity due to the effect of shear action [62].

Another potential type of shear failure that may affect blast-loaded elements is the *direct shear failure* [13], [51], as illustrated in Figure 2.13. This is a localized shear response that can appear at areas of discontinuity, such as the support area. This type of failure is typical of short-duration dynamic loads and is driven by high shear inertial forces. This failure occurs early in the structural response before any significant bending deformation takes place and thus it is not associated with flexure.

The failure that governs the response of the element depends on parameters inherent to the structure (e.g., resistance and stiffness, strain rate effects of materials, and *L/d* ratio) and the blast load (e.g., peak overpressure, rise time, and duration of the load). Magnusson et al. [63] describe that RC elements designed to fail under bending (when loaded statically) may instead develop shear failure if exposed to blast loading. This seems to be related to the rate of loading, as more impulsive loading may activate higher modes of vibration and thus a larger portion of the internal strain energy will be due to shear action rather than bending action.

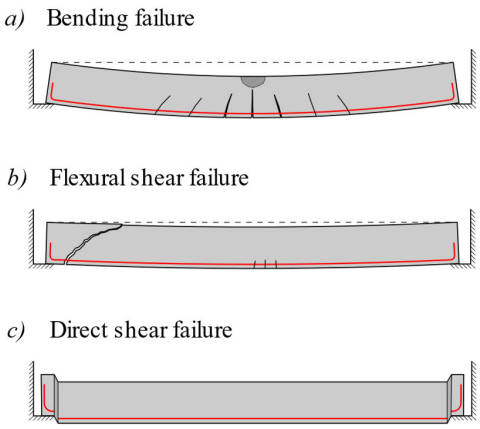

Figure 2.13. Typical failure modes of blast-loaded simply supported RC elements.

2.5.4 Simplified approach to evaluate the dynamic response

There exit several methods for determining the response of structural elements subjected to blast loading, ranging from simplified methods (such as those based on energy principles or on equivalent static loading) to advanced methods with numerical simulations with CFD codes (for simulation of blast waves) and finite element (FE) models (for evaluation of the dynamic response). However, in many cases, especially for design, it is sufficient with the estimation of the maximum response at critical points of the element (e.g., at midpoint). For this purpose, many structural elements can be represented by a simplified single-degree-of-freedom (SDOF) system, see Figure 2.14. In a SDOF system, the entire mass of the structure acts as a lumped centre of mass and the structural resistance is described as a function of the displacement of this centre. The total structural response can then be represented by the dynamic equation of motion, as given by Eq. (2.3), in which *m* is the mass of the RC element and *R(u)* is the resistance as a function of the displacement. The blast load is represented by a single forcing function *F(t)* that

acts on the centre of mass. The RC element can be converted into an equivalent SDOF system using transformation factors for mass (k_m), resistance (k_k) and load (k_F), see e.g., [51], [53].

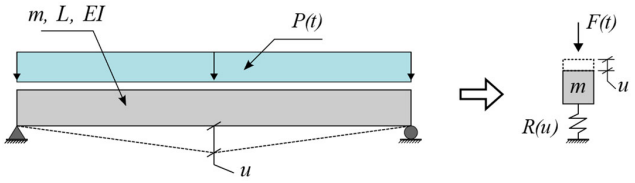

Figure 2.14. Beam subjected to a distributed transient load and equivalent SDOF system.

$$k_m m\ddot{u} + k_k R(u) = k_F F(t) \tag{2.3}$$

The relationship between the resistance offered by the structure and the corresponding displacement, *R(u)*, is usually described by an idealized ductile elastoplastic response, as shown in Figure 2.15. Here, R_M is the resistance to bending failure and $u_{M.d}$ is the maximum allowed deformation. The elastic portion extends from the origin to a theoretical yield point at a deformation u_{el}. The plastic portion is a line that extends horizontally from this yield point to failure. The failure criterium in the plastic domain is commonly specified by design codes as the rotational capacity at the support, θ_{pl}, which can be converted to the deformation capacity, $u_{M.d,}$ at the midpoint of the element. The part of the displacement corresponding to plastic deformation is not recoverable. Hence, it is a permanent structural damage. In this way, the displacement of the centre of mass of a structure is an indication of the damage caused by the imposed load. The deformation u_{tot} is the maximum deformation caused by load. Notice that the energy dissipated by the structure (internal work, W_i) is equivalent to the area under the resistance curve up to u_{tot}.

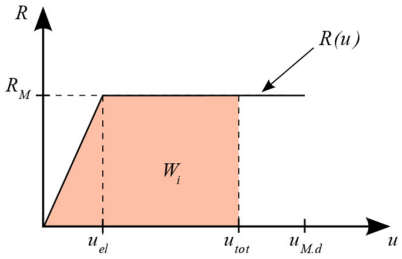

Figure 2.15. Idealized response of a RC beam failing under a ductile bending mechanism.

Different approaches can be used to solve a SDOF system. For simple structures subjected to simple pressure pulses, the equation of motion can be solved analytically. The solution to simple standard cases is also available in charts in multiple design guidelines and books, e.g., [53], [64]. For more advanced cases, numerical methods may be needed [65], [66]. Examples of such numerical methods include the Newmark β method [67] and the Central Difference method.

2.6 Uncertainties in design of RC elements

RC structures are affected by different sources of uncertainties. A large amount of research work aimed at understanding and quantifying uncertainties concerning RC structures is available in the literature, see e.g., [50], [68]–[71]. Three different types of uncertainties are

usually distinguished within the context of reliability of structures, namely: physical uncertainty, statistical uncertainty, and model uncertainty [72], [73]. Physical uncertainty refers to the natural variability of physical quantities. This includes loads and actions on the structures as well as material and geometrical properties. Statistical uncertainty emerges from incomplete statistical information, such as limited sample size. Finally, model uncertainty is the result of simplifications in the mathematical models used to relate a certain response variable (e.g., capacity) with a set of input variables (e.g., material strength, reinforcement amount, cross-section height) as well as neglected or unknown effects of the input variables.

In most practical applications, it is sufficient to represent the uncertainties with basic random variables with given probability distributions. Such basic random variables may correspond to the variables commonly used in conventional structural engineering, such as strength properties of concrete and reinforcement or cross-section height. The uncertainty related to a certain resistance model is represented by the random variable θ_R, which is the ratio between the actual resistance, R_{real}, and the predicted value of resistance calculated with the resistance model, $R_{model}(\boldsymbol{X})$, as given by Eq. (2.4). Here, the vector $\boldsymbol{X} = (X_1, X_2, \dots, X_n)$ contains the basic variables X_i for actions and structural properties.

$$\theta_R = \frac{R_{real}}{R_{model}(\boldsymbol{X})} \tag{2.4}$$

When describing uncertainties, it is desirable to use well-stablished probability distributions. For instance, the *normal distribution* is often used to represent the uncertainties related to the geometrical properties or material strength, while the *lognormal distribution* is traditionally used for describing model uncertainties [72]. The defining parameters of the probability distributions (e.g., mean, standard deviation) can be estimated based on statistical data from experiments [50].

3 Research Area I: Vapour cloud explosions on urban roads

3.1 Overview

The estimation of the blast loading from VCEs on urban roads that affects nearby structures is a difficult task. Unlike explosions caused by high explosive charges (such as TNT), the strength of a VCE may vary over a wide range depending on several factors such as confinement, congestion, mixture composition and concentration, and ignition location. This difficulty extends to the prediction of the blast loading generated by the VCE.

Different simplified methods to estimate the parameters of the free-field blast load from VCEs are available in the literature. Examples of such methods include the TNO Multi-Energy method (TNO-MEM), the Baker-Strehlow-Tang (BST) method, and the Congestion Assessment Method. In all these methods, the strength of the blast source is an essential input. Therefore, to accurately estimate the blast wave parameters from a VCE with such methods, the gas explosion scenario must be properly described first. Some guidelines and recommendations for the choice of the blast strength for different standard conditions can be found in the literature. However, such recommendations are mostly applicable for settings within the petrochemical industry. For other situations, such as gas explosions on roads, estimation of the source strength may be achieved by comparison against explosion experiments or aided by advanced numerical simulations.

Advanced numerical codes based on computational fluid dynamics (CFD) can be used to obtain relatively accurate predictions. However, CFD codes may be unsuitable for many situations due to high-cost and time demands. Furthermore, the knowledge required to properly handle such complex methods is usually outside the expertise of the wider community of structural engineers and risk analysts.

Considering that CFD calculations may be out of reach for many situations, and the fact that very few relevant experimental studies on gas explosions on roads are available in the literature, analysts and engineers today are forced to use their own experience and personal judgment to estimate the strength of VCEs on roads. However, considerable disparities in the prediction of blast parameters may stem from these assumptions. Therefore, this is a clear weakness of this type of simplified approach.

Based on this background, the work carried out within Research Area I aims at contributing towards the following research questions (repetition, see Section 1.2):

- **RQ1**: *What is the expected strength of vapour cloud explosions on urban roads?*
- **RQ2:** *What are the most relevant parameters affecting the strength of vapour cloud explosions on urban roads?*

The methodology and results of this part of the research were compiled in **Paper I**. In this chapter, a summary of the work accomplished is presented.

3.2 Research methodology

The approach chosen to meet the research questions concerning Research Area I is illustrated in Figure 3.1. The study was carried out with numerical simulations based on computational

fluid dynamics, and, where deemed necessary, comparison against published experiments was performed.

The work started with an extensive literature survey of the mechanisms of gas explosions and blast loads in urban environments. Furthermore, different CFD tools were investigated. The outcome of this stage, besides reviewing the state of the art, was to find a suitable tool to perform the calculations. Additionally, relevant gas explosion experiments were identified to perform in-house validation of the chosen CFD tool. The software FLACS-CFD [33] was selected. One of the reasons for this choice is the extended use and recognition of FLACS-CFD within the industry around the globe. Furthermore, several research studies dealing both with evaluation of gas explosion scenarios using FLACS-CFD and development and validation of the code are available in the literature.

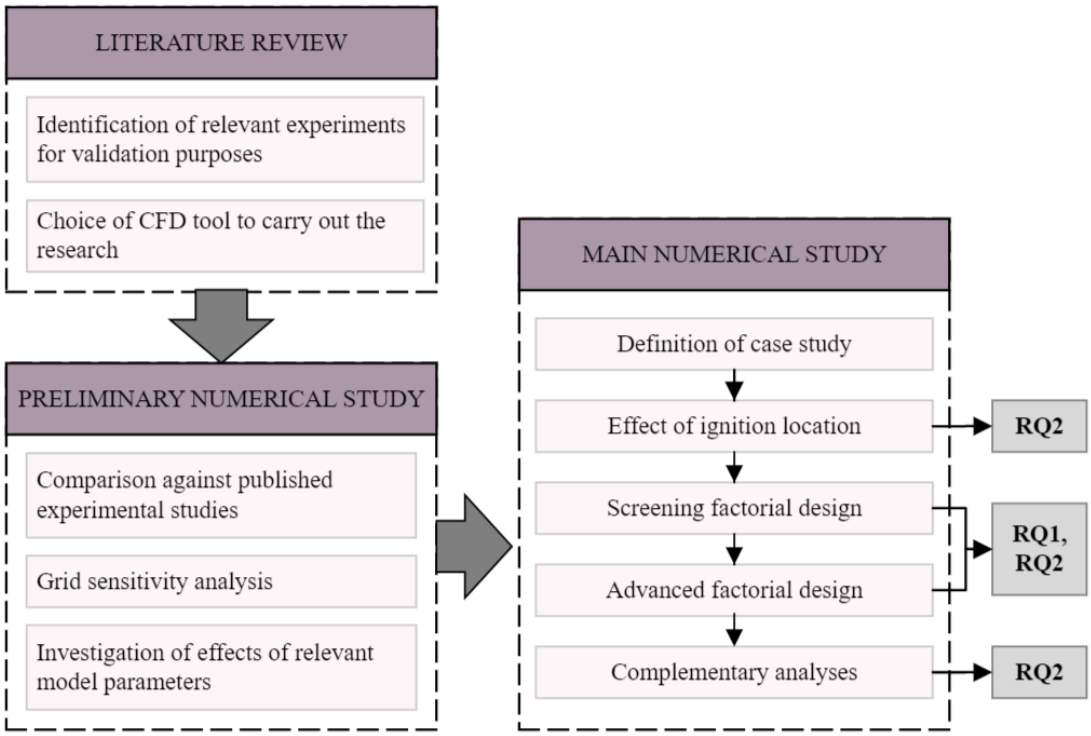

Figure 3.1. Research methodology for the work conducted in Research Area I.

The simulation work initiated with a series of preliminary studies aimed at validating the chosen tool and finding out the appropriate modelling technique and model parameters for the conditions at hand. Initially, a grid sensitivity analysis was conducted. In this stage, strong grid-dependency in FLACS-CFD was identified. For that reason, comparison against gas explosion experiments was carried out with the purpose of selecting an appropriate grid cell size. Based on this comparison, it was concluded that six grid cells in the region under the vehicle provided reasonable results. This led to a grid cell size of **50 mm**, which was used for all models in the main numerical study. Furthermore, it was found that the initial turbulence conditions may have a significant effect on scenarios with relatively low congestion and confinement levels. Thus, another outcome of this stage was the choice of initial turbulence conditions for the scenarios of interest.

The main study of this work started with the design of the case study, which consisted of several scenarios with a group of vehicles on a road engulfed by a premixed gas cloud. Several

simplifications such as the shape and concentration of the gas cloud and the geometry of the vehicles were implemented. The setup and geometry of the studied cases were designed with the intention to allow for potential future experimental replication. The geometry of the mock-up vehicle appears in Figure 3.2.

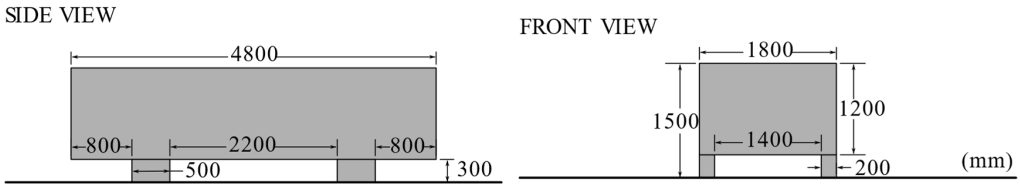

Figure 3.2. Geometry of mock-up vehicle.

A schematic representation of the gas cloud and the configuration of the group of vehicles is presented in Figure 3.3. The studied scenarios were described in terms of six parameters:

- ***A***: Distance between vehicles.
- ***B***: Extension of the gas cloud in the horizontal plane outside the group of vehicles, measured from the edge of the bounding box of the group of vehicles.
- ***C***: Height of the gas cloud, measured from the ground.
- ***D***: Number of vehicles in the transversal direction (*y*-direction in Figure 3.3).
- ***E***: Number of vehicles in the longitudinal direction (*x*-direction in Figure 3.3).
- ***F***: Location of the ignition point.

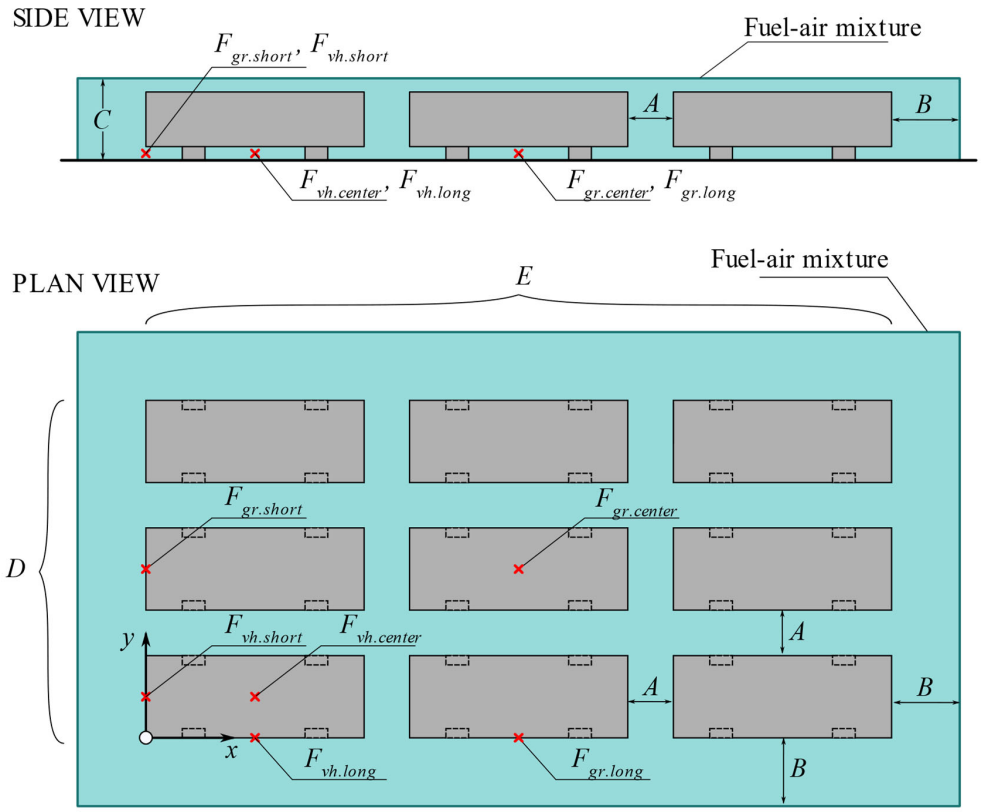

Figure 3.3. Parameters defining the studied gas explosion scenarios.

A picture of a sample model in FLACS-CFD appears in Figure 3.4. The calculation domain was divided into a *core domain* (with constant grid cell size of 50 mm) and a *stretched domain* (cells are stretched gradually from the core domain out to the boundaries). All vehicles and the unburned gas cloud were modelled within the core domain. Only results within this domain are considered relevant. Ideally, combustion of the gas cloud should occur entirely inside the core domain. Indeed, care was taken to ensure that combustion in the *positive* x- and y-direction happened entirely within the core domain. However, due to high computational demands of the models, the core domain was reduced in the *negative* x- and y-direction. The stretched domain fulfils the purpose of attenuating the impact of the boundary conditions on the results in the core domain. All boundaries, apart from the ground, were modelled as non-reflective boundary conditions.

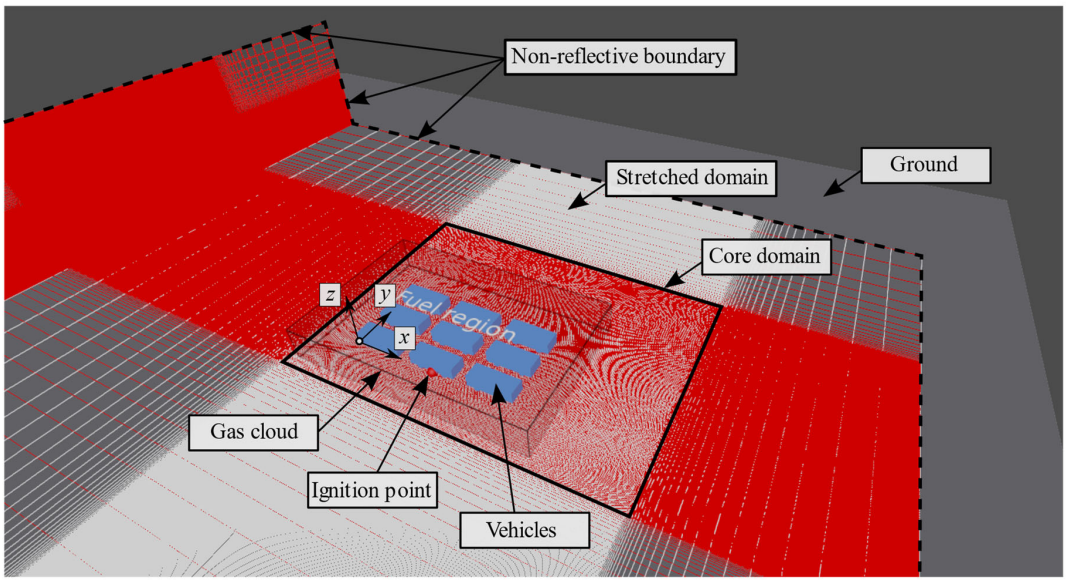

Figure 3.4. Example of a model with 3×3 vehicles in FLACS-CFD.

An important decision made during the design of the case study was the choice of gas type. Due to the heavy computational requirements, it was decided to evaluate only one type of gas. Therefore, only mixtures of *propane* and air with a *stochiometric concentration* were used. Propane was chosen as it appears to be the most transported flammable gas in Sweden and often constitutes the basis for risk analysis in the country [18], [19].

In the main study stage, the principles of factorial designs were implemented in two stages to carry out a parametric study with a practical amount of computational resources. Initially, a screening 2^{6-1} fractional factorial design with the six basic defining parameters at two levels each was carried out. In this factorial design, 32 combinations of factors (commonly referred to as *runs*) were analysed. The levels for each factor in this design appear in Table 3.1. The four most significant factors emerging from this screening analysis were later evaluated with a 3^{4-1} fractional factorial design. The levels for each factor in the 3^{4-1} fractional factorial design appear in Table 3.2. In this design, 27 runs were carried out. The different runs for each factorial design are described in **Paper I**. In total, 53 runs were evaluated with the factorial designs (six scenarios appear in both factorial designs).

It should be noted that an additional analysis prior to the factorial runs was required in order to determine the levels concerning the location of the ignition point (factor *F*). Furthermore, a complementary analysis to investigate the influence of the shape of the wheels was carried out after the factorial analysis was completed.

Table 3.1. Factors and levels used in the 2^{6-1} fractional factorial design.

Factor	Description	Low (-)	High (+)	Unit
A	Distance between vehicles	0.5	1.5	m
B	Extension of the cloud in the horizontal plane outside the group of vehicles	0.0	4.0	m
C	Height of the cloud	1.8	3.6	m
D	Number of vehicles in the transversal direction	1	3	-
E	Number of vehicles in the longitudinal direction	1	3	-
F	Location of the ignition point	$F_{vh.short}$	$F_{gr.long}$	-

Table 3.2. Factors and levels used in the 3^{4-1} fractional factorial design.

Factor*	Parameter	Low (0)	Medium (1)	High (2)	Unit
A	Distance between vehicles	0.5	1.5	2.5	m
B	Extension of the cloud in the horizontal plane outside the group of vehicles	0.0	2.0	4.0	m
C	Height of the cloud	1.8	2.7	3.6	m
D	Number of vehicles in the transversal direction	1	2	3	-

* For all runs: $E = 3$ and $F = F_{gr.long}$

3.3 Results

3.3.1 Explosion overpressure

The focus of the work presented in **Paper I** was the strength of vapour cloud explosions in open traffic environments. In other words, the main output of interest was the maximum overpressure at the main source of blast.

For the scenarios studied here, in which the gas mixture consisted of equivalent stochiometric clouds of propane and air, the values of maximum overpressure ranged between 2 kPa and 106 kPa. This corresponds to strength class 2 to 7 in the TNO-MEM (see Figure 2.8). The maximum overpressure values obtained for all scenarios are summarized in Figure 3.5. The 25th percentile and 75th percentile of the data are approximately 8 kPa and 35 kPa. Notice that values of overpressure greater than 100 kPa were obtained only for one scenario, in which all parameters were set at their high value[5]. Indeed, about 90% of all scenarios produced overpressure values lower than 50 kPa (strength class 6).

[5] Factor *A* was set to 1.5 m, which is the high level in the 2^{6-1} design, but the medium level in the 3^{4-1} design.

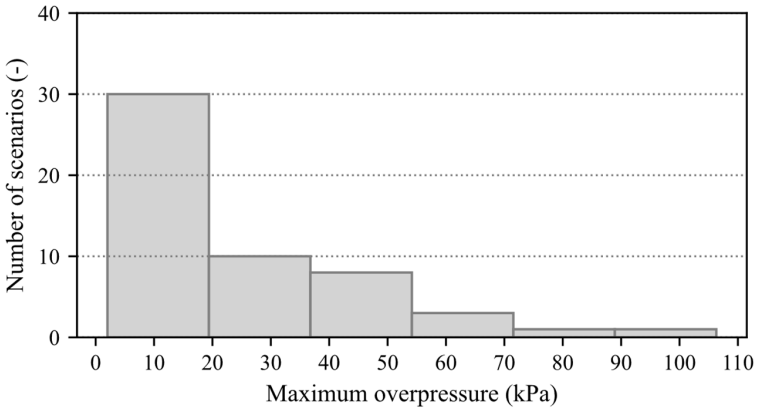

Figure 3.5. Distribution of maximum overpressure obtained from the studied scenarios.

The results show that while explosion strength greater than 50 kPa may occur for the environment of interest, this appears to happen only for a few cases under the most unfavourable conditions considered in this study. Furthermore, it was found that such high explosion strength only developed in a localized area with a relatively small source radius (in relation to the size of the congested region), meaning that the energy contributing to this strength was relatively limited in comparison with the total gas inventory. This can be observed in the contour plot of peak overpressure for the most critical scenario (run 1-32) in Figure 3.6. Here, it is evident that high overpressure values arise in a local area outside the group of vehicles, opposite the location of the ignition point. The localized stronger explosion outside the group of vehicles is an indication of acceleration of the flame and pressure build-up as the flame travels through the congested and confined region. Furthermore, turbulence on the wake of the group of vehicles appears to have an important role in combustion just outside the group of vehicles.

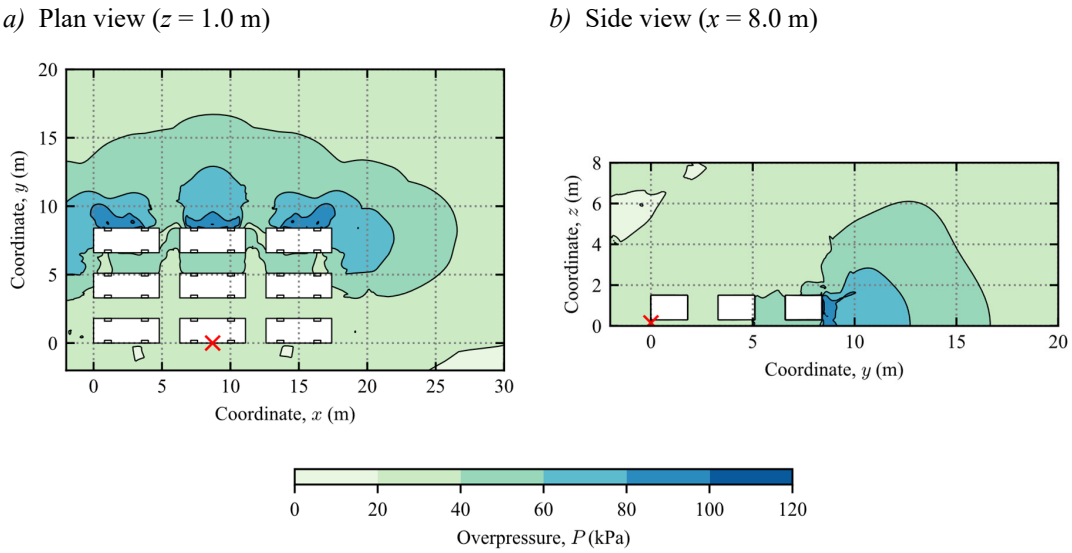

Figure 3.6. Contour plot of peak overpressure for run 1-32 based on the numerical simulations. P_{max} = 106 kPa. Defining parameters: A = 1.5 m, B = 4.0 m, C = 3.6 m, D = 3, E = 3, F = $F_{gr.long}$.

In contrast, weaker explosions in general showed a more symmetrical pattern of distribution of peak overpressure. In some cases, pressure decay followed a nearly hemispherical distribution, as shown in Figure 3.7 for run 1-29.

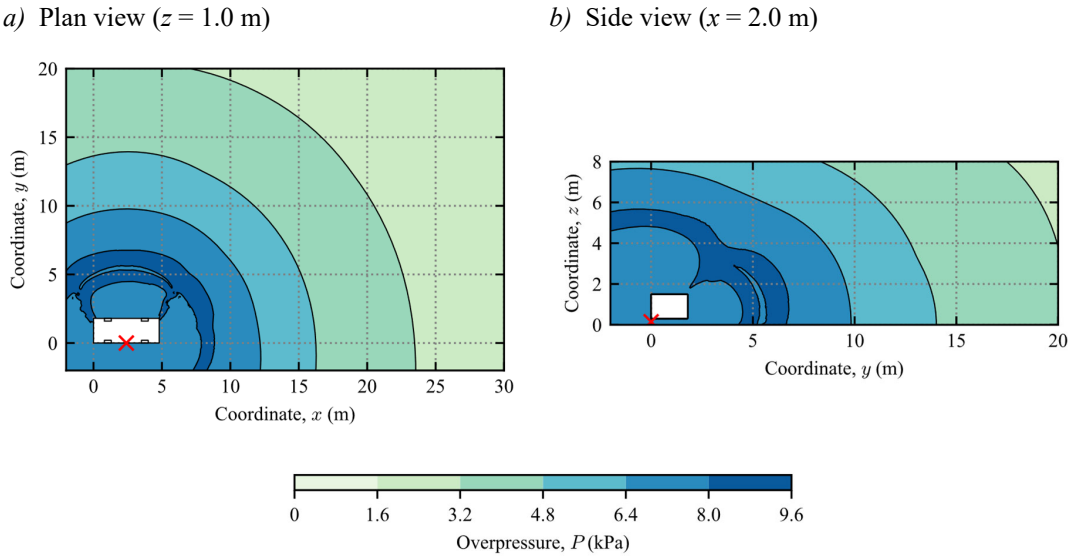

Figure 3.7. Contour plot of peak overpressure for run 1-29 based on the numerical simulations. P_{max} = 9 kPa. Defining parameters: A = 1.5 m, B = 4.0 m, C = 3.6 m, D = 1, E = 1, F = $F_{gr.long}$.

The combustion products at different times after ignition at a height of 0.2 m (i.e., under the vehicles) are presented in Figure 3.8 for run 1-32. Plots of combustion products can be used to follow the evolution of the flame front. From visual inspection, it is apparent that the flame speed increased as the flame traversed the congested region. This shows that the chosen modelling approach was able to capture flame acceleration due to effects such as confinement and flame folding around obstacles.

The pressure-time histories at different monitor points for runs 1-29 and 1-32 are presented in Figure 3.9. For each run, the selected monitor points were located along the same line (parallel with the *y*-axis). Notice that the rise time to peak overpressure was shorter for the stronger explosion, resembling the general shape for pressure waves in Figure 2.6(b). On the other hand, for the weaker explosion, the overpressure increased gradually over a longer time, and the resulting pressure-time history exhibited a similar general shape to that of acoustic waves in Figure 2.6(c). Furthermore, pressure decay (both in distance and time) occurred more rapidly for the stronger explosion.

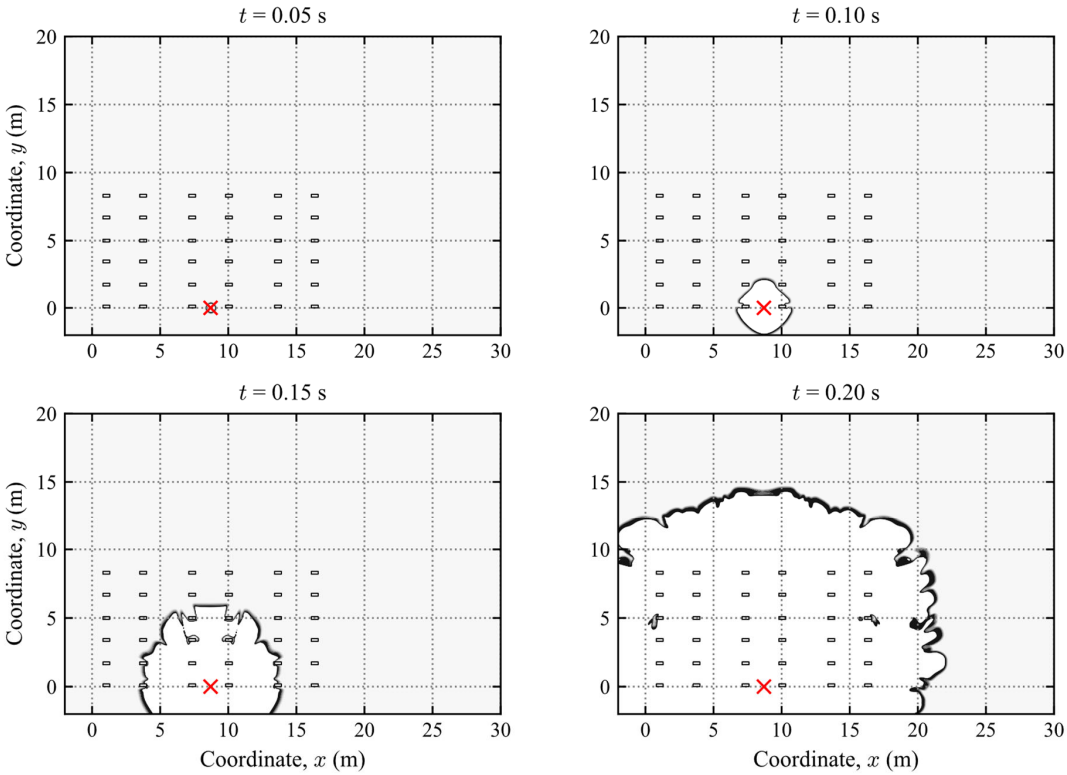

Figure 3.8. Flame front development in run 1-32 based on the numerical simulations.

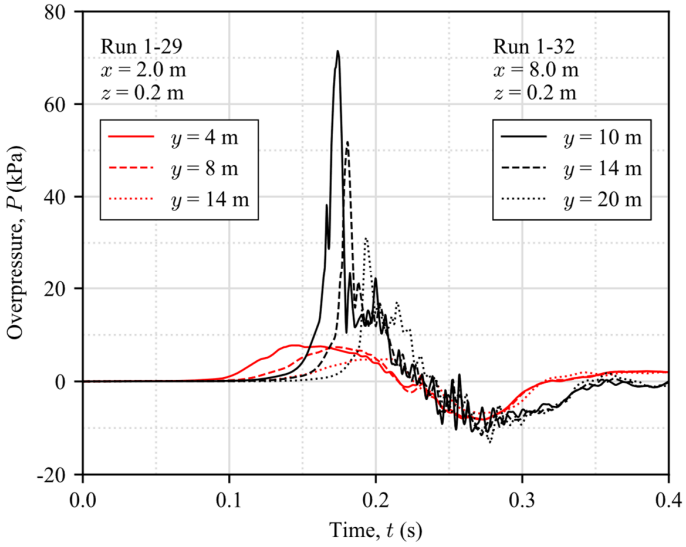

Figure 3.9. Pressure-time history at different monitor points along selected paths for runs 1-29 and 1-32 based on the numerical simulations.

3.3.2 Parametric study

The most significant factors and interaction of factors affecting the strength of the VCEs according to the screening 2^{6-1} factorial design are presented in Figure 3.10. The figure gives the estimate of the *effect* of the most important factors and interactions, which is an indication of the influence that changing one factor would have on the explosion strength. The results show that the most significant parameter was the number of vehicles in the transversal direction (factor *D*). That is, increasing the number of vehicles in the transversal direction results in greater peak overpressure values. This is probably due to the increase in flame travel length in confined and congested conditions provided by additional vehicles. Furthermore, from the analysis of the results, it also became apparent that the shape of the wheels in relation to the main direction of flame travel had an important role in the significance of factor *D*.

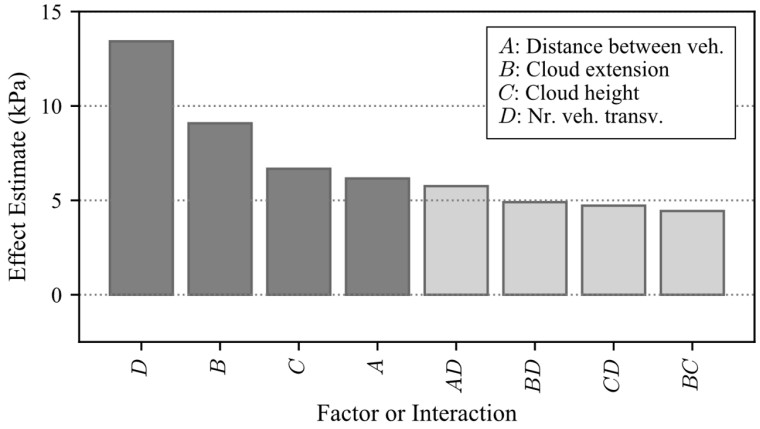

Figure 3.10. Most significant effects arising from the 2^{6-1} factorial design. Main effects in dark shade. Interaction effects in light shade.

Besides factor *D*, factors A, *B*, and *C* as well as their interaction with factor *D* were also found to have an important influence on the resulting maximum overpressure caused by the VCE. For this reason, these four factors were evaluated more thoroughly in the subsequent 3^{4-1} factorial design. The main effects of the four factors from the 3^{4-1} factorial design appear in Figure 3.11.

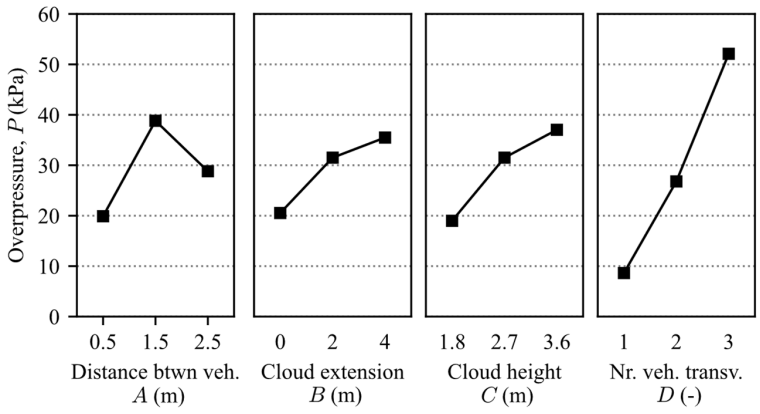

Figure 3.11. Main effects obtained from the 3^{4-1} fractional factorial design.

The factors associated with the dimensions of the gas cloud (factors *B* and *C*) were observed to have a positive effect on the peak overpressure. However, the influence of these factors seemed to decrease as the level of the factors increased. This suggests that pressure enhancement subsides after a certain critical gas volume and further increase in gas volume will not lead to significant increase in overpressure. This may be connected to a recirculation zone with high turbulence behind the group of vehicles. If there is unburned gas available to fill in the recirculation zone, higher overpressure will be generated when the flame front reaches this zone. However, turbulence will gradually fade out further away from the congested region, which entails that high flame speeds cannot be maintained.

The separation distance between vehicles (factor *A*) was shown to have a significant non-linear effect. It appears that, up to a certain critical value, increasing this distance had the effect of increasing the flame travel length while maintaining critical turbulence levels which boosted flame acceleration and pressure build-up. However, increasing *A* beyond the critical value seems to lead to flame speed decay as the relief of pressure in the region between vehicles becomes more significant. It is reasonable to assume that this critical distance depends on the geometry of the vehicle.

The number of vehicles in the longitudinal direction (factor *E*) had the least influence of all parameters studied. In scenarios with a predominantly rectangular layout with the long side in the longitudinal direction, the attenuating effects of side relief appeared to dominate over the enhancement of flame acceleration due to the longer travel path provided by the elongated geometry. However, the number of vehicles in the longitudinal direction may gain more relevance if the dimension of the congested region in the longitudinal direction is similar or smaller than the dimension in the transversal direction.

Finally, a clear effect was observed for the position of the ignition point (factor *F*). The location of ignition influenced both the charge strength and the amount of energy contributing to blast generation. The ignition point is a multidimensional parameter associated with side relief, flame travel length, direction of flame travel, and obstacle shape. For the studied cases, edge ignition caused the greatest value of overpressure when the flame front travelled mainly in the transversal direction. However, edge ignition also produced the weakest explosion for situations in which flame travel occurred mainly in the longitudinal direction. Centre ignition appears to produce intermediate values of maximum overpressure. However, in general, the influence of the position of ignition on the explosion strength was found to be less significant than that of other factors.

The direction and shape of the wheel in relation to the direction of flame travel was suspected to have a strong influence. As this relates to the most significant parameter identified here, it was decided to perform a follow-up analysis to test this hypothesis. Explosion scenarios inside a flat channel both without any obstacle inside and with obstacles with three different shapes (similar to the conditions in the region under the vehicles) were numerically evaluated with FLACS-CFD. This is described in **Appendix A**. The results show that the presence of obstacles led to greater overpressure than a case without any obstruction. An increase in overpressure (in relation to the unobstructed case) of about 50% was observed for rectangular objects oriented parallel to the main flow. However, for square objects and rectangular objects placed perpendicularly to the flow, the enhancement was of about 140%. Clearly, the position and shape of the wheel in relation with the main direction of flow will have an impact on the explosion strength.

4 Research Area II: Risk of shear failure of blast-loaded RC structures

4.1 Overview

Reinforced concrete (RC) slabs subjected to blast loads are primarily designed to dissipate energy by means of large inelastic deformations, rather than relying on large load resistance. This means that brittle shear failure with limited deformation capacity must be avoided. Therefore, ensuring that the RC slabs fail under a ductile bending mechanism enabling high energy absorption capacity is a key aspect of blast-resistant design.

The design shear force commonly used during design of blast-loaded RC slabs corresponds to the shear force in the critical section when the element has reached its maximum bending resistance. This means that the design shear force is a function of the bending resistance, not of the applied blast load. That is, increasing the bending resistance of the slab will increase the requirements regarding shear resistance.

However, due to uncertainties involved in the design of blast-loaded structures, it may be difficult to calculate the real bending and shear resistance of the element. This makes determining the governing failure mode difficult. Such uncertainties stem from the statistical variation of material properties and geometry, simplifications and unknowns in the resistance models, and the use of the lower characteristic values of material properties and partial safety factors in the current design standards.

Several research studies regarding shear behaviour of blast-loaded RC elements are available in the literature. For instance, Magnusson et al. [63] investigated the influence of the characteristics of the load (e.g., peak load and rise time) and the structural wave propagation on the shear behaviour of blast-loaded RC beams. Some studies regarding the influence of shear effects on the moment capacity of statically and dynamically loaded RC structures are also available, see e.g., [51]. However, no research concerning the effects of uncertainties in the interaction between shear resistance and bending resistance is available in the literature, to the knowledge of the author.

Hence, there is a risk for brittle shear failure developing in elements intended to fail under ductile bending due to the uncertainties involved in the design process. Based on this, the work done within Research Area II seeks to meet the following research questions (repetition, see Section 1.2):

- **RQ3:** *What is the likelihood of brittle shear failure in blast-loaded slender RC one-way slabs considering the uncertainties related to the material properties, geometry, and resistance models?*
- **RQ4:** *How can the confidence level regarding ductile failure of blast-loaded slender RC one-way slabs be increased?*

The methodology and results of this part of the research project are presented in **Paper II**. This chapter gives a summary of the work carried out. It is worth highlighting that an additional goal of this work is to raise awareness about the influence of uncertainties on the failure mode of blast-loaded RC elements. Therefore, to present the topic in a concise manner, some simplifications were intentionally implemented.

4.2 Research methodology

The strategy chosen to carry out the work within Research Area II concerning the effects of the uncertainties associated with the failure of RC slabs subjected to blast loading was a combination of simplified analytical models with the Monte Carlo method. The work was structured as shown in Figure 4.1.

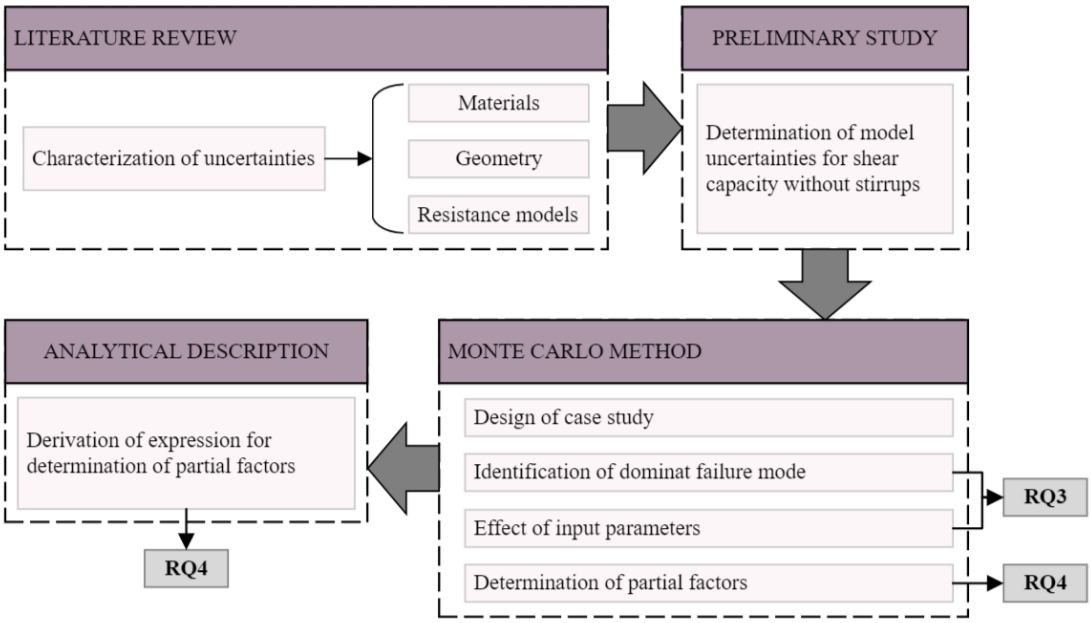

Figure 4.1. Research methodology for the work conducted in Research Area II.

The study initiated with a literature review. The goal of this stage was to identify relevant sources of uncertainties concerning the moment and shear capacity of RC elements. The resistance models in Eurocode 2 were adopted. Furthermore, suitable probability density functions for the most relevant uncertainties were extracted from the literature. The uncertainty connected to the following variables were deemed the most relevant:

- Material properties: Concrete compressive strength, f_c; yield strength of longitudinal reinforcement, f_y; yield strength of shear reinforcement, f_{yw}.
- Geometrical properties: Error of the effective depth of the cross-section, Δd
- Resistance models: Bending capacity, M_R; shear capacity without stirrups, V_{Rc}; shear capacity with stirrups, V_{Rs}.

From the literature review, it became apparent that the uncertainty distribution of the model for shear capacity without stirrups was much sensitive to the geometrical conditions and reinforcement amount of the RC elements. For that reason, it was decided to describe the distribution of this model uncertainty by performing a comparison against the ACI-DAfStb database [74], considering only those specimens in the database that had similar characteristics to the elements studied here. Goodness-of-fitness tests were performed on several probability distributions with the purpose of identifying the most suitable.

The dynamic increase factors (DIFs) for the material properties were assumed to be 1.0 in this study. One reason for this choice is the fact that the DIF values specified in design standards, such as UFC 3-340-02 [64], have an added safety margin for shear failure, which would distort the study carried out here. Furthermore, a DIF value of 1.0 is currently commonly used in Sweden [59].

The case study consisted of 32 simply supported RC one-way *strips* of slabs with varying dimensions and reinforcement amounts. The specimens were divided into two groups of 16 specimens each. The specimens in one the groups did not have any shear reinforcement, while the slabs in the other group had the minimum amount of shear reinforcement required by Eurocode 2. The slabs were assumed to be subjected to a uniformly distributed blast load. A schematic representation of the geometrical conditions of the specimens appears in Figure 4.2. All studied slabs are slender elements according to the definition in [75]. That is, only specimens with a slenderness (L/d) greater than 9.6 were evaluated.

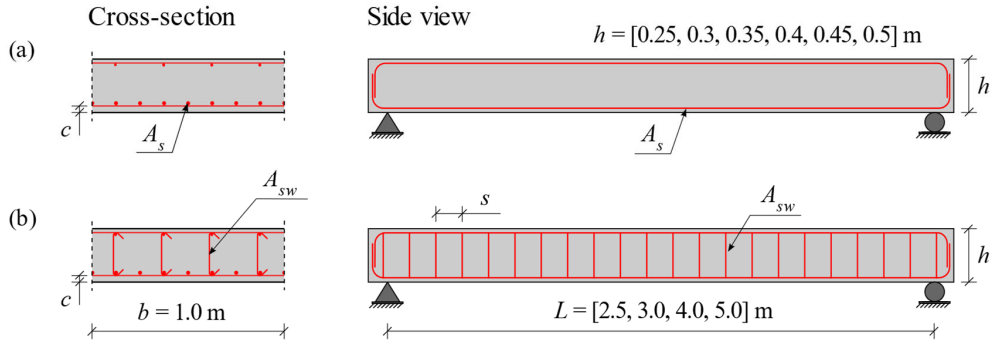

Figure 4.2. Geometry conditions of case study: a) geometry and reinforcement layout of the slabs without stirrups, b) geometry and reinforcement layout of the slabs with stirrups.

The problem was formulated as a limit state function, G, defined by Eq. (4.1).

$$G = R/E \tag{4.1}$$

In Eq. (4.1), R is the *resistance* to shear failure while E is the *effect* of the action. In this case, the *effect* was given by the equivalent resistance to bending failure. In the context of this work, the resistance is equal to the total load at failure, and was determined using Eq. (4.2) and (4.3), in which $q_{R.V}$ is the equivalent distributed static load at shear failure, and $q_{R.M}$ is the equivalent distributed static load at bending failure.

$$R = q_{R.V} \cdot L \tag{4.2}$$

$$E = q_{R.M} \cdot L \tag{4.3}$$

The reinforcement amounts of the studied specimens were selected so that the *design*[6] resistance to shear failure was theoretically equal to the *design* resistance to bending failure.

[6] Here, the term *design* means that characteristic material properties and partial factors for materials were used.

This means that the starting point for the study was specimens with a *balanced* design that fulfils $G = 1$.

Both R and E are random variables due to the uncertainties related to the materials, geometry, and resistance models. Thus, the limit state variable G inherits the random nature from R and E. Using Monte Carlo method with $N = 10^5$ iterations, the distribution of G was determined for all studied specimens. From Eq. (4.1), it is evident that shear failure would be the dominant failure mode in those cases in which $G < 1$ (i.e., the resistance to shear failure is the lowest). Conversely, bending failure would govern failure of the slab in cases in which $G > 1$. Therefore, the determination of the probability of *premature shear failure* can be achieved by solving Eq. (4.4), in which n is the number of iterations in which the criterion $G < 1$ is met.

$$P_f = P\{G < 1\} = n/N \tag{4.4}$$

Moreover, an iterative procedure with the Monte Carlo method was followed to determine values of an additional partial factor, γ_V, to increase the design shear force according to Eq. (4.5). The purpose was to provide a way to improve the confidence level regarding the desired failure mode.

$$V_{Rd} \geq \gamma_V \cdot V_{Ed} \tag{4.5}$$

The work was further complemented with analytical derivation of the partial factors with the objective of verifying the results from the Monte Carlo approach. Furthermore, an analytical expression could be helpful for easy calculation of the required partial factors for different input parameters or for finding new values of partial factors for different target reliability levels.

4.3 Results

Before performing the Monte Carlo simulations, it was necessary to describe the uncertainty associated with the model for shear capacity without stirrups in Eurocode 2. This was done by comparing experimental data in the ACI-DAfStb shear database [74] against predictions with the resistance model. The database was filtered to consider only those test specimens with similar characteristics to those of the specimens studied in this work. The ratio between the actual capacity of the RC beams in the database and the theoretical capacity according to the resistance model is shown in Figure 4.3(a). This ratio corresponds to the model uncertainty, θ_{VRc}, according to Eq. (2.4). Different probability density functions (PDFs) were fitted to the data. The results showed that the Burr XII distribution was the most suitable for describing the probabilistic distribution of θ_{VRc}, see Figure 4.3(b). However, the lognormal distribution is traditionally used for representing model uncertainties in the literature. For that reason, both distributions were used in the main study of this part of the thesis to represent θ_{VRc}.

a) Model uncertainty vs *d* for studied sample

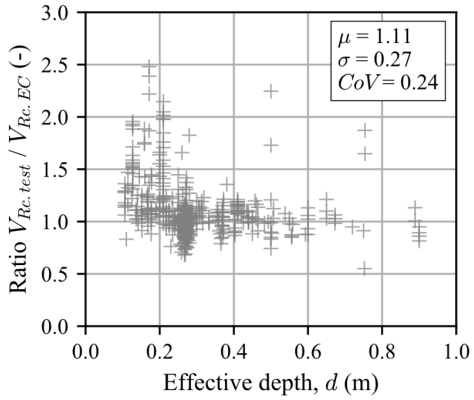

b) Fitting of different PDFs to the data

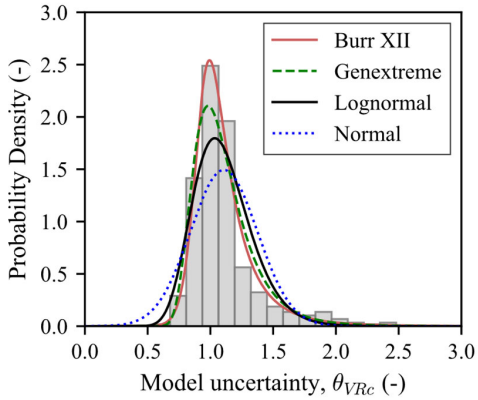

Figure 4.3. (a) Experimental data concerning model uncertainty associated with shear capacity without stirrups [74]. (b) fitting of various probability density functions (PDFs).

The Monte Carlo method was initially implemented on a reference specimen with h = 300 mm and L = 3000 m. Figure 4.4 gives the distribution of the limit state variable for the specimen without stirrups, G_c, and with stirrups, G_s. The calculations for the specimen without stirrups were performed twice: assuming both the Burr XII and lognormal distribution for the uncertainty related to the shear capacity model. However, only the results for the calculations with the Burr XII distribution appear in Figure 4.4.

a) Uncertainty distribution for G_c

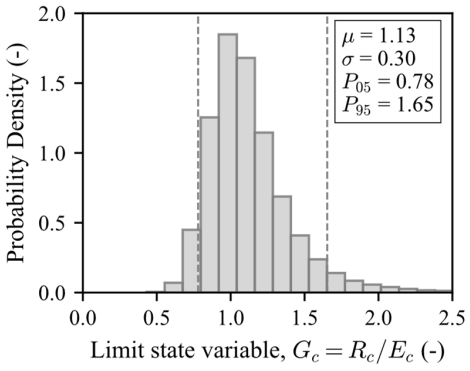

b) Uncertainty distribution for G_s

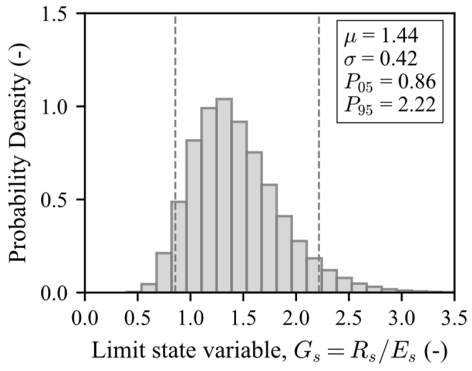

Figure 4.4. Uncertainty distribution of the limit state variable for a reference specimen with h = 300 mm and L = 3.0 m: (a) specimen without stirrups, G_c; (b) specimen with stirrup, G_s. The results for the specimen without stirrups are for the case in which the Burr XII distribution was used for the uncertainty of the shear capacity model.

The calculated probability of premature shear failure for the reference element without shear reinforcement was $P_{f.c}$ = 36%. Approximately the same probability of shear failure was obtained regardless of which distribution was used to describe the uncertainty of the shear capacity model. That is, both the Burr XII and lognormal distribution were found to be equally suitable to

estimate the probability of shear failure of elements without shear reinforcement. For the element with shear reinforcement, the calculated probability of shear failure was $P_{f.s}$ = 13%. Therefore, bending failure appears to be the most likely failure mode for elements initially designed for a balanced failure. This is perhaps not a surprising outcome considering that only *slender* elements were studied. Furthermore, the confidence level was higher for elements with shear reinforcement. The results also showed that the uncertainty associated with the shear capacity models had the most significant influence on the probability of shear failure from among the sources of uncertainty considered.

To investigate the influence of slenderness (L/d) on the results, the same calculations were repeated for all specimens in the sample. It was found that the mean value of G showed a minor decrease as the slenderness increased. Consequently, the probability of shear failure exhibited a slight increase as the slenderness increased, as presented in Figure 4.5. That is, the risk of premature shear failure appears to be greater for the more slender elements. Notice that P_f became as large as 44% for elements without stirrups, and as large as 15% for specimens with stirrups.

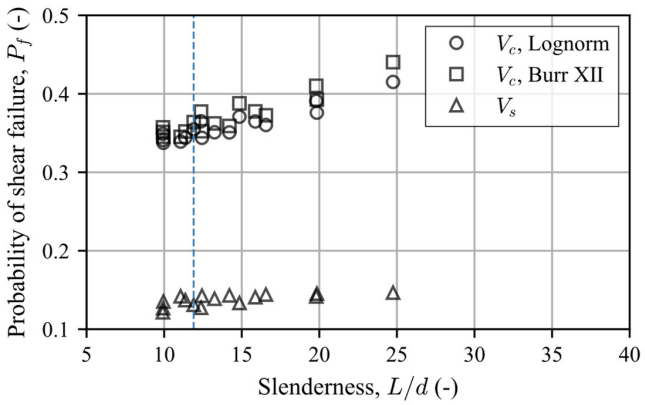

Figure 4.5. Variation of the probability of shear failure, P_f, as a function of the slenderness of the specimen. The dashed vertical line represents the position of the reference element with h = 300 mm, L = 3000 mm, and L/d = 11.9.

Even though bending was found to be the most likely failure mode for the studied specimens, the calculated probability of shear failure may still be considered unacceptable, particularly for elements without stirrups. This because the consequences of a brittle shear failure are likely to be more severe than that of bending failure. A potential strategy to increase the confidence level of the desired failure mode is to introduce an additional partial factor during the design process. Such a factor could be used to increase the design shear force to achieve a given target reliability level. The curves in Figure 4.6 represent the values of this partial factor as a function of the target probability of shear failure, which were determined using the Monte Carlo method. Notice that the choice of probability distribution function to represent the model uncertainty seems to influence the calculated partial factor. In particular, using the lognormal distribution to describe the model uncertainty may lead to more conservative partial factors for elements without shear reinforcement.

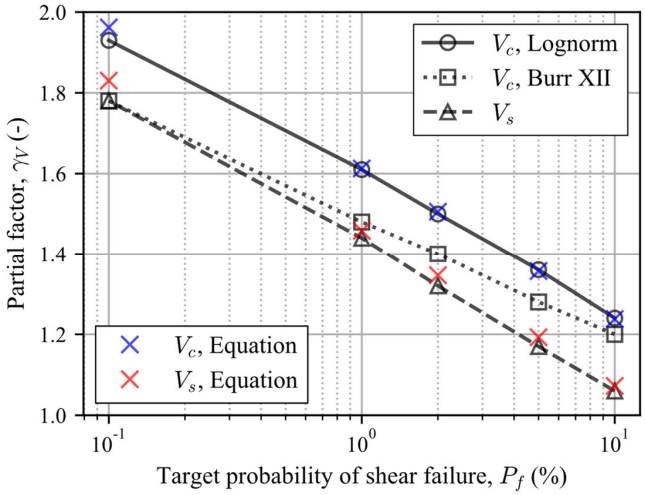

Figure 4.6. Calculated partial factors to reduce risk of shear failure at different target probability of premature shear failure without stirrups (V_c) and with stirrups (V_s). The crosses represent values calculated with the analytical expression given by Eq. (B13).

The partial factors were also determined analytically in **Appendix B**. The main goal was to verify the results with the Monte Carlo method. In this derivation, it was assumed that *R* and *E* were lognormally distributed. Therefore, the derived expressions are less accurate for cases in which the model uncertainty for shear resistance without stirrups is represented by the Burr XII (or other distribution). Figure 4.6 also gives a comparison between the partial factors determined with the Monte Carlo method and the partial factors calculated with Eq. (B13). Remarkably good agreement was found for the cases in which the lognormal distribution was used. However, for the stricter targets of probability of shear failure, Eq. (B13) seems to give slightly greater values for the partial factor than those determined with the Monte Carlo method. Nevertheless, the good correspondence is an indication that the results obtained with the Monte Carlo method are reasonable.

5 Conclusions and future research

5.1 Conclusions

Due to the increase in risk for accidental gas explosions in urban environments, blast-resistant design of reinforced concrete (RC) structures may become a common requirement in modern urban development. The increase of this risk is associated with densification of urban areas located in proximity to roads in which hauling of flammable gases is allowed and the advent of vehicles powered by alternative fuels.

Explosion hazards related to loss of containment of flammable gases have been a major concern for several decades within the petrochemical industry and substantial experience and knowledge has been accumulated during the years. However, extrapolation of this experience to urban settings is not always straightforward. Furthermore, the wider structural engineer community may lack the necessary competences regarding both determination of the explosion and blast loads and the dynamic response of structures subjected to them. This means that successful and optimal implementation of blast-resistant design of urban RC structures remains a challenging task.

The work presented in this thesis contributes towards expanding the knowledge concerning different aspects related to explosion hazards in urban centres. Two key research areas were identified. One of them deals with the strength of vapour cloud explosions (VCEs) on urban roads. The other area is concerned with the uncertainties related to the failure mode of blast-loaded RC slabs.

Today, the determination of the strength of VCEs in urban settings is an important source of subjectivity and disparity within the construction industry in Sweden. In this thesis, the strength of explosions of mixtures of *propane* and air in urban settings was investigated aided by advanced computational fluid dynamics (CFD) calculations. The work started with the definition of standard scenarios with varying traffic configuration, dimension of gas cloud, and location of the ignition point. The expected strength of the gas explosions for the studied conditions was found to range between 2 kPa and 100 kPa. For strong explosions, the large values of overpressure were obtained in a localized area, which suggests that the combustion energy contributing to strong blast generation was limited in relation to the total available energy.

The influence of different parameters defining the explosion scenarios on the resulting strength was also investigated. The number of vehicles in the transversal direction was shown to have the most significant effect: increasing the number of vehicles resulted in greater overpressure. This was probably due to longer flame travel distance across the congested and partly confined region, but also due to the influence of the shape of the wheels. On the other hand, the number of vehicles in the longitudinal direction had the least significant influence among the studied parameters.

By properly describing the gas explosion in terms of strength and combustion energy, it is possible to use simplified methods to determine the blast loading affecting structures nearby the gas explosion. The results gathered in this work opened avenue for future recommendations for choice of the strength class, which is an important input to simplified methods such as TNO Multi-Energy method (TNO-MEM) and the Baker-Strehlow-Tang (BST) method. Given the

strength class, the parameters of the blast load produced by VCEs that impinges on nearby structures can be determined from blast charts. For instance, the results suggest that strength class between 2 and 7 in the TNO-MEM is expected for the conditions studied in this work, depending on the combination of the input parameters.

RC elements subjected to such blast loading are primarily designed to dissipate the energy imposed by the loading by large plastic deformations. Hence, preventing premature brittle shear failure is essential during the design of blast-loaded RC elements. To achieve a proper level of confidence regarding the preferred failure mode, it is beneficial to understand the effects of uncertainties associated with materials, geometry, and resistance models. This is the focus of the work performed under the second key research area. The Monte Carlo method was implemented to calculate the probability of premature shear failure of simply supported RC one-way slabs considering such uncertainties. Identifying the most significant parameters affecting the calculated probability was also part of the study.

The results showed that bending failure was the most likely failure mode of RC slabs initially designed for a balanced failure (i.e., the design resistance to shear and bending failure are theoretically equal). Depending on the slenderness (L/d) of the element, the calculated probability of premature shear failure, P_f, varied between 34% and 44% for RC slabs without shear reinforcement and between 12% and 15% for RC slabs with shear reinforcement. In general, the probability of shear failure was larger for increasing slenderness ratio. The uncertainties related to the resistance models were found to have the most significant effect on the probability of shear failure, over the influence of the material and geometrical uncertainties.

Whether this probability of shear failure is acceptable or not depends on the risk tolerability for a given design. Indeed, considering that the potential consequences of shear failure may be much more severe than those of bending failure for the same level of loading, the calculated probability of shear failure may still be relatively large. This work put forward an additional partial factor, γ_V, to increase the design shear force with the aim to improve the confidence level regarding the preferred failure mode. Such partial factor depends on the target reliability level. The partial factor was shown to be dependent on the probability distribution function used for representing the model uncertainties. For elements without shear reinforcement, the calculated partial factor varied from 1.24 for $P_f \leq 10\%$ to 1.93 for $P_f \leq 0.1\%$. For elements with shear reinforcement, the partial factor ranged between 1.06 for $P_f \leq 10\%$ and 1.78 for $P_f \leq 0.1\%$. Note that for lower slenderness ratio (L/d), using this partial factor may render slabs without shear reinforcement unsuitable, as it may not be possible to meet the augmented shear capacity requirements without shear reinforcement.

5.2 Suggestions for future research

Investigation of the specific impulse of blast waves generated by VCEs is a logical continuation of the work carried out in this thesis. The specific impulse is connected to the amount of combustion energy that contributes to blast generation. In the TNO-MEM, this parameter is related to the volume of the source of strong blast within the gas cloud. Therefore, to produce complete recommendations for using the method for evaluation of gas explosions on urban roads, it is necessary to study the specific impulse in relation to the volume of gas participating in the generation of strong blast.

Furthermore, investigation of the effects of gas reactivity on the strength of VCEs on roads would be beneficial. The work carried out here used only propane-air mixture. Propane is a gas

with a medium reactivity that has been used in the past as a reference for reactivity scaling. Thus, evaluating the possibility of extending the results obtained here for other gases by means of reactivity scaling would be of interest.

The arrangement and size of obstacles within the cloud are known to influence VCEs. The wheel shape was also found to have a significant impact on the resulting explosion pressure. For this reason, it would be beneficial to study gas explosion scenarios on roads in which the placement of the vehicles is irregular (e.g., random placement of the vehicles) and/or with vehicles of varying size and shape.

It would also be of interest to investigate the mechanisms of propagation of blast waves in urban environments with the aim of developing simplified approaches to account for phenomena like shielding and channelling.

Using more advanced methods that allow to consider a more realistic distribution of shear forces in blast-loaded RC slabs in a probabilistic study will probably be needed to confirm the results obtained here. Furthermore, including the strain rate effects on the material properties would be favourable. However, this would require a statistical description of the uncertainties associated with the strain rate effects.

The ultimate capacity and the deformation limit of RC structures may be significantly enhanced by tensile membrane action. Therefore, it would be beneficial to investigate the positive effects of membrane forces on blast-loaded RC structures and how they can be accounted for in simplified calculation methods.

Furthermore, the part of the research dealing with the response of RC structures so far focused on single elements. Hence, it would be of interest to study the behaviour of structural systems consisting of interconnected elements subjected to internal and external explosion loads.

References

[1] Polismyndigheten, "Sprängningar och skjutningar," *polisen.se*. https://polisen.se/link/4c9c6642003b48ac947dd3107370731c (accessed Jul. 02, 2023).

[2] E. Planas, E. Pastor, J. Casal, and J. M. Bonilla, "Analysis of the boiling liquid expanding vapor explosion (BLEVE) of a liquefied natural gas road tanker: The Zarzalico accident," *Journal of Loss Prevention in the Process Industries*, vol. 34, pp. 127–138, Mar. 2015, doi: 10.1016/j.jlp.2015.01.026.

[3] S. Lyu, S. Zhang, X. Huang, S. Peng, and J. Li, "Investigation and modeling of the LPG tank truck accident in Wenling, China," *Process Safety and Environmental Protection*, vol. 157, pp. 493–508, Jan. 2022, doi: 10.1016/j.psep.2021.10.022.

[4] E. N. Bjarsell, "Rätt tätt - en idéskrift om förtätning av städer och orter." Boverket, 2016.

[5] M. Johansson, A. Ansell, M. Hallgren, and J. Leppänen, "Inventering av kunskapsbehov i byggbranschen med hänsyn till explosioner i en förtätad stadsmiljö (Inventory of knowledge needs in the construction industry regarding explosions in densified urban environments)," Chalmers University of Technology, Göteborg, Rapport ACE 2020:16, 2020.

[6] A. From and G. Wiberg, "Kompletterande händelserapport: Brand i biogasbuss, Klaratunneln (Accident report: Fire in a biogas bus, Klaratunneln)," Storstockholms brandförsvar, 360–277/2019, Mar. 2019.

[7] J. Ekström, "Blast and impact loaded concrete structures: Numerical and experimental methodologies for reinforced plain and fibre concrete structures," Ph.D. Thesis, Chalmers University of Technology, Gothenburg, 2017.

[8] M. Johansson, "Structural behaviour in concrete frame corners of civil defence shelters: Non-linear finite element analyses and experiments," Ph.D. Thesis, Chalmers University of Technology, Gothenburg, 2000.

[9] J. Leppänen, "Concrete structures subjected to fragment impacts," Ph.D. Thesis, Chalmers University of Technology, Gothenburg, 2004.

[10] U. Nyström, "Modelling of concrete structures subjected to blast and fragment loading," Chalmers University of Technology, Gothenburg, 2013.

[11] M. Plos, "Application of fracture mechanics to concrete bridges. Finite element analyses and experiments," Ph.D. Thesis, Chalmers University of Technology, Gothenburg, 1995.

[12] H. Hansson, "Warhead penetration in concrete protective structures," Lic. Thesis, KTH Royal Institute of Technology, Stockholm, 2011.

[13] J. Magnusson, "Shear in concrete structural elements subjected to dynamic loads," Ph.D. Thesis, KTH Royal Institute of Technology, Stockholm, 2019.

[14] D. Bjerketvedt, J. R. Bakke, and K. van Wingerden, "Gas explosion handbook," Gexcon, Bergen, 1992.

[15] Center for Chemical Process Safety, *Guidelines for vapor cloud explosion, pressure vessel burst, BLEVE, and flash fire hazards*, 2nd ed. Hoboken, NJ, USA: John Wiley & Sons, Inc., 2010. doi: 10.1002/9780470640449.

[16] G. Purdy, “Risk analysis of the transportation of dangerous goods by road and rail,” *Journal of Hazardous Materials*, vol. 33, no. 2, pp. 229–259, Feb. 1993, doi: 10.1016/0304-3894(93)85056-K.

[17] Publication Series on Dangerous Substances, “PGS 3: Guidelines for quantitative risk assessment [’Purple book’],” 2005.

[18] O. Alvarsson and J. Jansson, “Jämförelsestudie av riskbedömningar avseende vägtransport av farligt gods (Comparison study of risk analyses regarding road transport of hazardous materials),” M.Sc. thesis, Lund University, Lund, 2016.

[19] E. Dahlen, “Inventory of knowledge needs, with regard to explosion loading, in a densified urban environment.,” M.Sc. thesis, Chalmers University of Technology, Gothenburg, 2019.

[20] Räddningsverket, “Värdering av risk,” P21-182/97, 1997.

[21] M. Johansson, “Luftstötvåg (Blast waves in air),” MSB448, 2012.

[22] N. Kubota, *Propellants and explosives: Thermochemical aspects of combustion*, 3rd ed. Wiley-VCH, 2015.

[23] G. Chamberlain, E. Oran, and A. Pekalski, “Detonations in industrial vapour cloud explosions,” *Journal of Loss Prevention in the Process Industries*, vol. 62, p. 103918, Nov. 2019, doi: 10.1016/j.jlp.2019.103918.

[24] E. S. Oran, G. Chamberlain, and A. Pekalski, “Mechanisms and occurrence of detonations in vapor cloud explosions,” *Progress in Energy and Combustion Science*, vol. 77, p. 100804, Mar. 2020, doi: 10.1016/j.pecs.2019.100804.

[25] C. J. M. van Wingerden, “Experimental study of the influence of obstacles and partial confinement on flame propagation, Part II,” TNO Prins Maurits Laboratory, EUR 9541 EN/II, 1984.

[26] B. Hjertager, K. Fuhre, and M. Bjørkhaug, “Spherical gas explosion experiments in a high-density obstructed 27 m3 corner,” Chr. Michelsen institute, Bergen, 1988.

[27] C. J. M. van Wingerden, J. G. Visser, and H. J. Pasman, “Combustion in obstructed diverging and non-diverging flow fields,” in *Combustion and Reaction Kinetics*, Karlsruhe, 1991.

[28] C. J. Lea and H. S. Ledin, “A Review of the state-of-the-art in gas explosion modelling,” Health and Safety Laboratory, HSE HSL/2002/02, 2002.

[29] D. J. Park and Y. S. Lee, “A comparison on predictive models of gas explosions,” *Korean J. Chem. Eng.*, vol. 26, no. 2, pp. 313–323, Mar. 2009, doi: 10.1007/s11814-009-0054-5.

[30] M. Johansson, “Beräkningsstöd: Gasexplosion i det fria (Gas explosions in the open),” Myndigheten för samhällsskydd och beredskap, B06-105, Dec. 2017.

[31] J. S. Puttock, M. R. Yardley, and T. M. Cresswell, “Prediction of vapour cloud explosions using the SCOPE model,” *Journal of Loss Prevention in the Process Industries*, vol. 13, no. 3, pp. 419–431, May 2000, doi: 10.1016/S0950-4230(99)00045-5.

[32] B. Hjertager, O. Sæter, and T. Solberg, *Numerical modelling of gas explosions - A review*. 1996.

[33] Gexcon AS, “FLACS-CFD v22.1 User’s Manual.” Apr. 27, 2022.

[34] J. Puttock, F. Walter, D. Chakraborty, S. Raghunath, and P. Sathiah, "Numerical simulations of gas explosion using Porosity Distributed Resistance approach Part −1: Validation against small-scale experiments," *Journal of Loss Prevention in the Process Industries*, vol. 75, p. 104659, Feb. 2022, doi: 10.1016/j.jlp.2021.104659.

[35] S. V. Patankar and D. B. Spalding, "A Calculation procedure for the transient and steady-state behaviour of shell-and-tube heat exchangers," in *N.H. Afgan and E.V. Schhinder (eds.), Heat Exchangers: Design and Theory Sourcebook*, New York: McGraw-Hill, 1974, pp. 155–176.

[36] J. Geng, T. Mander, and Q. Baker, "Blast wave clearing behavior for positive and negative phases," *Journal of Loss Prevention in the Process Industries*, vol. 37, pp. 143–151, Sep. 2015, doi: 10.1016/j.jlp.2014.10.018.

[37] R. Benintendi, Ed., *Process Safety Calculations*, 2nd ed. Elsevier, 2021.

[38] A. C. van den Berg, "The multi-energy method: A framework for vapour cloud explosion blast prediction," *Journal of Hazardous Materials*, vol. 12, no. 1, Art. no. 1, Dec. 1985, doi: 10.1016/0304-3894(85)80022-4.

[39] Q. A. Baker, M. J. Tang, E. A. Scheier, and G. J. Silva, "Vapor cloud explosion analysis," *Process Safety Progress*, vol. 15, no. 2, pp. 106–109, 1996, doi: 10.1002/prs.680150211.

[40] M. J. Tang and Q. A. Baker, "A new set of blast curves from vapor cloud explosion," *Process Safety Progress*, vol. 18, no. 4, pp. 235–240, 1999, doi: https://doi.org/10.1002/prs.680180412.

[41] J. S. Puttock, "Fuel gas explosions guidelines: the Congestion Assessment Method.," 1995.

[42] K. G. Kinsella, "A rapid assessment methodology for the prediction of vapour cloud explosion overpressure.," presented at the International conference and exhibition on safety, health and loss prevention in the oil, chemical and process industries, Singapore, 1993.

[43] J. B. M. M. Eggen, "GAME: Development of guidance for the application of the multi-energy method," TNO Prins Maurits Laboratory, HSE CRR 202/1998, 1998.

[44] R. Pitblado, J. Alderman, and J. K. Thomas, "Facilitating consistent siting hazard distance predictions using the TNO Multi-Energy Model," *Journal of Loss Prevention in the Process Industries*, vol. 30, pp. 287–295, Jul. 2014, doi: 10.1016/j.jlp.2014.04.010.

[45] G. F. Kinney and K. J. Graham, *Explosive Shocks in Air*. Berlin, Heidelberg: Springer Berlin Heidelberg, 1985. doi: 10.1007/978-3-642-86682-1.

[46] O. S. Isaac, O. G. Alshammari, E. G. Pickering, S. D. Clarke, and S. E. Rigby, "Blast wave interaction with structures – An overview," *International Journal of Protective Structures*, p. 20414196221118596, Sep. 2022, doi: 10.1177/20414196221118595.

[47] M. Johansson and L. Laine, "Bebyggelsens motståndsförmåga mot extrem dynamisk belastning. Delrapport 2: Explosion i gatukorsning (The resistance of housing settlements subjected to extreme dynamic loading, Part 2: Explosion in street crossing)," Myndigheten för samhällsskydd och beredskap, Karlstad, MSB450, 2012.

[48] A. Ratcliff, S. Rigby, S. Clarke, and S. Fay, "A Review of blast loading in the urban environment," *Applied Sciences*, vol. 13, no. 9, Art. no. 9, Jan. 2023, doi: 10.3390/app13095349.

[49] M. Johansson and L. Laine, "Bebyggelsens motståndsförmåga mot extrem dynamisk belastning. Delrapport 1: Last av luftstötvåg (The resistance of housing settlements

subjected to extreme dynamic loading, Part 1: Blast waves in air)," Myndigheten för samhällsskydd och beredskap, Karlstad, MSB449, 2012.

[50] R. Hingorani, "Acceptable life safety risks associated with the effects of gas explosions on reinforced concrete structures," Ph.D. Thesis, Universidad Politécnica de Madrid, 2017. doi: 10.20868/UPM.thesis.47772.

[51] T. Krauthammer, *Modern protective structures*. Taylor & Francis Group, 2008.

[52] M. Johansson and L. Laine, "Bebyggelsens motståndsförmåga mot extrem dynamisk belastning, Del 3: Kapacitet hos byggnader (The resistance of housing settlements subjected to extreme dynamic loading, Part 3: Capacity of buildings)," Myndigheten för samhällsskydd och beredskap, Karlstad, MSB 0142-10, 2012.

[53] J. M. Biggs, *Introduction to structural dynamics*. McGraw-Hill, 1964.

[54] D. Cormie, G. Mays, and P. Smith, *Blast effects on buildings*, 3rd Edition. London: ICE Publishing, 2020.

[55] P. H. Bischoff and S. H. Perry, "Compressive behaviour of concrete at high strain rates," *Materials and Structures*, vol. 24, no. 6, pp. 425–450, Nov. 1991, doi: 10.1007/BF02472016.

[56] L. J. Malvar and C. A. Ross, "Review of strain rate effects for concrete in tension," *Materials*, vol. 95, pp. 735–739, 1998.

[57] M. Johansson and R. Rempling, "Design of impulse loaded concrete structures: a comparison of FKR 2011 with various design regulations," Chalmers University of Technology, Gothenburg, Report 2016-16, 2016. doi: 10.13140/RG.2.2.10757.29924.

[58] CEN, "EN 1992-1-1:2004. Eurocode 2: Design of concrete structures - Part 1-1: General rules and rules for buildings." European Committee for Standardisation (CEN), Brussels, 2004.

[59] Fortifikationsverket, "Fortifikationsverkets konstruktionsregler FKR 2011 (Swedish Fortifications Agency Building Regulations)," Eskilstuna, Dnr 4535/2011, 2011.

[60] E. G. Nawy, *Reinforced concrete: A fundamental approach*, 5th Edition. Prentice Hall, 2003.

[61] Y. Yang, "Shear behaviour of reinforced concrete members without shear reinforcement: A new look at an old problem," Ph.D. Thesis, TU Delft, 2014.

[62] T. Krauthammer and W. J. Hall, "Modified Analysis of Reinforced Concrete Beams," *Journal of the Structural Division*, vol. 108, no. 2, pp. 457–475, Feb. 1982, doi: 10.1061/JSDEAG.0005881.

[63] J. Magnusson, M. Hallgren, and A. Ansell, "Shear in concrete structures subjected to dynamic loads," *Structural Concrete*, Mar. 2014, doi: 10.1002/suco.201300040.

[64] DOD, "UFC 3-340-02. Structures to resist the effects of accidental explosions." US Department of Defence (DOD), Washington, D.C., 2008.

[65] T. Krauthammer, N. Bazeos, and T. J. Holmquist, "Modified SDOF analysis of RC box-type structures," *Journal of Structural Engineering*, vol. 112, no. 4, pp. 726–744, Apr. 1986, doi: 10.1061/(ASCE)0733-9445(1986)112:4(726).

[66] T. Krauthammer, A. Assadi-Lamouki, and H. M. Shanaa, "Analysis of impulsively loaded reinforced concrete structural elements—I. Theory," *Computers & Structures*, vol. 48, no. 5, pp. 851–860, Sep. 1993, doi: 10.1016/0045-7949(93)90507-A.

[67] N. M. Newmark, “A method of computation for structural dynamics,” *Transactions of the American Society of Civil Engineers*, vol. 127, no. 1, pp. 1406–1433, Jan. 1962, doi: 10.1061/TACEAT.0008448.

[68] H. Baji, “The effect of uncertainty in material properties and model error on the reliability of strength and ductility of reinforced concrete members,” Ph.D. Thesis, The University of Queensland, 2014. doi: 10.14264/uql.2015.95.

[69] M. G. Stewart, “Reliability-based design and robustness for blast-resistant design of RC buildings,” *Advances in Structural Engineering*, vol. 25, no. 7, pp. 1402–1412, May 2022, doi: 10.1177/13694332221087341.

[70] D. E. Allen, “Statistical study of the mechanical properties of reinforcing bars,” p. 22 p., 1972, doi: 10.4224/40000624.

[71] D. E. Allen, “Probabilistic Study of Reinforced Concrete in Bending,” *JP*, vol. 67, no. 12, pp. 989–995, 1970, doi: 10.14359/7333.

[72] JCSS, “JCSS Probabilistic Model Code. Part 1: Basis of Design.” Zurich: Joint Committee on Structural Safety, 2001. [Online]. Available: www.jcss.byg.dtu.dk

[73] P. Thoft-Christensen and M. J. Baker, *Structural reliability theory and its applications*. Springer-Verlag Berlin Heidelberg, 1982.

[74] K.-H. Reineck and B. Fitik, *ACI-DAfStb databases 2020 with shear tests on structural concrete members without stirrups - Volume 1: Part 1 to Part 2.5*. Berlin: DAfStb, 2022.

[75] K.-H. Reineck, E. C. Bentz, B. Fitik, D. A. Kuchma, and O. Bayrak, “ACI-DAfStb database of shear tests on slender reinforced concrete beams without stirrups,” *SJ*, vol. 110, no. 5, pp. 867–876, Sep. 2013, doi: 10.14359/51685839.

Appendix A: Investigation of the influence of the shape of obstacles on the explosion overpressure

Numerical simulations with FLACS-CFD were used to investigate the effect of the shape of obstacles on the strength of a deflagration of a confined stoichiometric mixture of propane and air. Four scenarios in a 2D environment confined between two parallel horizontal plates were studied. Three of the scenarios had two objects within the confined region, while the remaining scenario had no obstruction. The geometry of the scenarios is presented in Figure A.1 and Figure A.2. The geometry was chosen to be representative of the characteristics of the flow in the region under vehicles. The distance between the confining plates was set to 300 mm, which is the same ground clearance assumed for the vehicles in the study described in **Paper I**. The dimensions of the gas cloud were set to 4.1×3.0×0.3 m.

Three different obstacles shapes were studied:

- Rectangular shape with dimensions 200×500 mm, with the long side *parallel* with the longitudinal direction of the channel. See Figure A.1(a) and Figure A.2(a).
- Rectangular shape with dimensions 200×500 mm, with the long side *perpendicular* to the longitudinal direction of the channel. See Figure A.1(b) and Figure A.2(b).
- Square shape with dimensions 500×500 mm. See Figure A.1(c) and Figure A.2(c).

The ignition point was placed at one edge of the gas cloud. The monitor point from which results are extracted was located in the opposite direction at 3.5 m from the centre of the gas cloud.

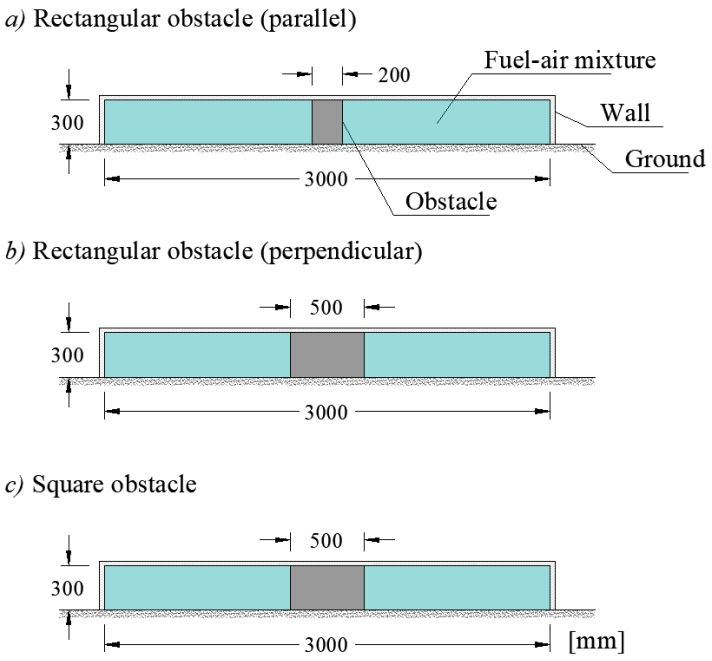

Figure A.1. Front view of the geometry of the 2D scenarios for evaluating the influence of the wheel shape.

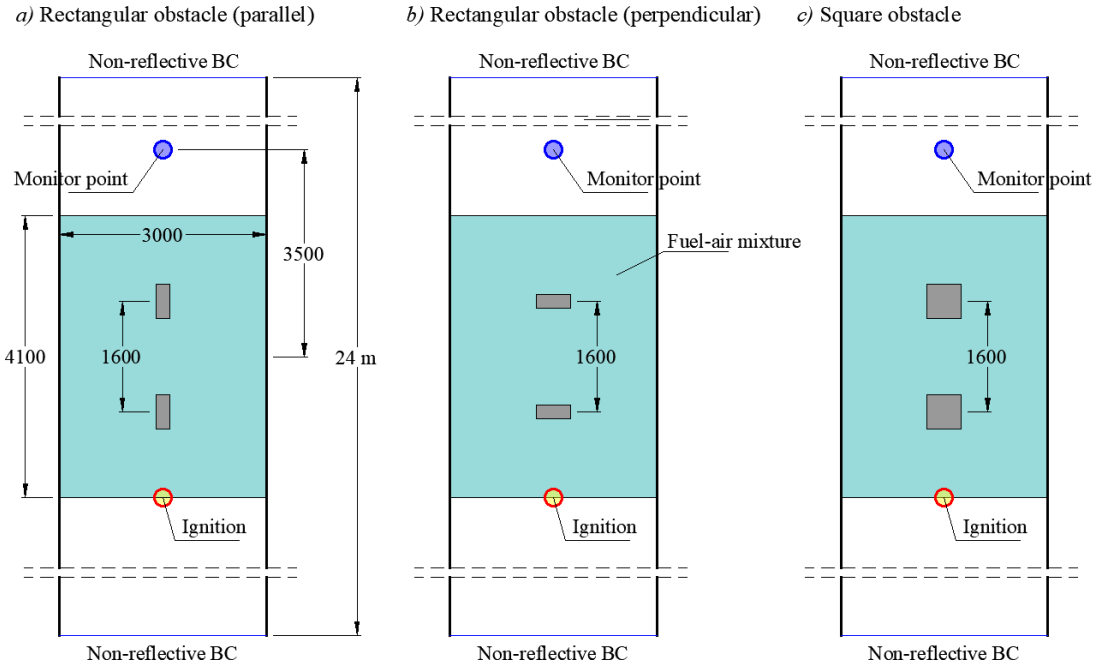

Figure A.2. Plant view of the geometry of the 2D scenarios for evaluating the influence of the wheel shape.

A grid cell size of **50 mm** was used over the entire domain. Non-reflective boundary conditions were used at the far ends of the channel, while reflective boundary conditions (walls) were used in all other boundaries. A picture of a sample model in FLACS-CFD appears in Figure A.3.

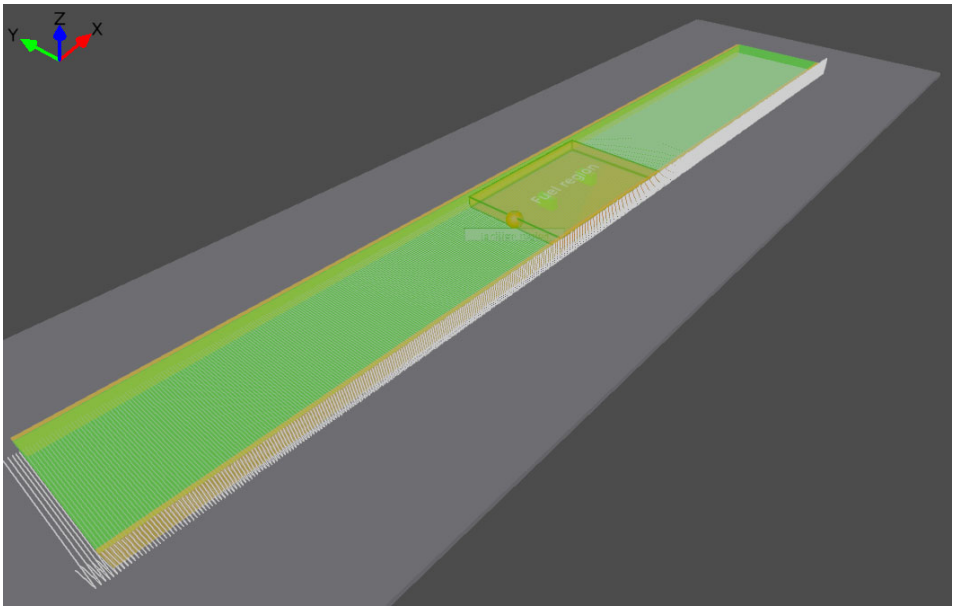

Figure A.3. Sample model of the numerical experiment in FLACS-CFD

Figure A.4 gives the results at the monitor point in the form of curves of overpressure over time. Notice that the case without obstruction gave the lowest value of peak overpressure (approximately 46 kPa). In contrast, the case with the rectangular object placed perpendicularly to the flow and the case with the square object produced peak overpressure values greater than 100 kPa. The case with the rectangular object placed parallel to the flow generated an intermediate value of peak overpressure (approximately 70 kPa).

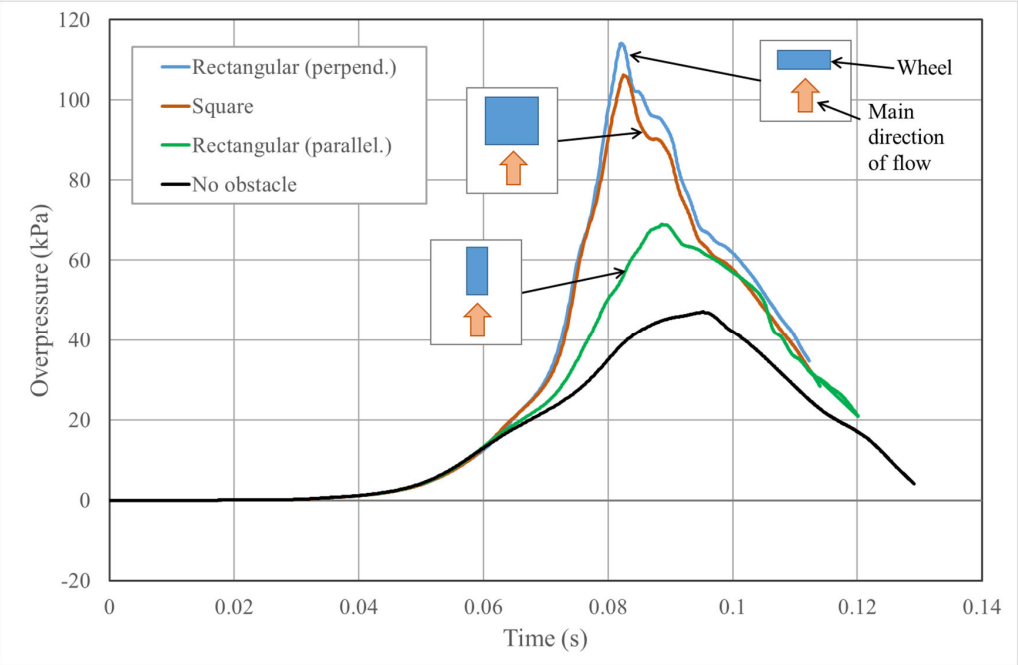

Figure A.4. Pressure-time history at the monitor point for all cases.

Appendix B: Analytical determination of additional partial factor for the design shear force in blast-loaded RC slabs.

An analytical procedure was followed to determine the partial factor γ_V aimed at increasing the confidence level regarding ductile failure in blast-loaded RC slabs. This derivation serves the purpose of verifying the results of the Monte Carlo simulations described in **Paper II**. The derivation is done under the assumption that both the resistance, R, and effect, E, can be described with the *lognormal distribution*. That is, the *Burr XII distribution* is not treated in this appendix. The analytical calculations are based on the semi-probabilistic method in Annex C in Eurocode 0. According to Eurocode 0, the safety verification is performed according to the following equations:

$$R_d \geq E_d \tag{B1}$$

$$R_d = \phi_R \mu_R \geq E_d = \gamma_E \mu_E \tag{B2}$$

Where E_d is the design value of the effect and R_d is the corresponding design value of the resistance. The parameter μ_R and μ_E are the mean values of R and E. The factors ϕ_R and γ_E are the partial factors for the resistance and effect respectively. Observe that E_d and R_d are not necessarily equal to V_{Rd} and V_{Ed}. Assuming lognormal distributions, the partial factors can be calculated according to the following expressions:

$$\phi_R \approx e^{-\alpha_R \cdot \beta \cdot CoV_R} \tag{B3}$$

$$\gamma_E \approx e^{-\alpha_E \cdot \beta \cdot CoV_E} \tag{B4}$$

Where α_R and α_E are the FORM sensitivity factors, and β is the desired target reliability index. The factors α_R and α_E may be taken as 0.8 and -0.7, respectively, according to Eurocode 0. It should be noticed that these expressions are generally accepted for situations where $CoV \leq 0.2$, which is the case for the distribution of E. However, the distribution of R has a coefficient of variation larger than 0.2 for both cases (without and with shear reinforcement). For the sake of simplicity, it was nonetheless decided to proceed with the simplified expressions.

The factors ϕ_R and γ_E are combined into a factor γ_G in Eq. (B5). The factor γ_G can then be calculated according to Eq. (B6).

$$\mu_R \geq \frac{\gamma_E}{\phi_R} \mu_E = \gamma_G \cdot \mu_E \tag{B5}$$

$$\gamma_G \approx e^{(-\alpha_E \cdot \beta \cdot CoV_E + \alpha_R \cdot \beta \cdot CoV_R)} \tag{B6}$$

To relate Eq. (B5) with Eq. (4.5) , it is necessary to express the design shear resistance, V_{Rd}, and design shear force, V_{Ed}, in terms of the mean values of R and E (i.e., μ_R and μ_E):

$$\mu_R \approx \mu_{\theta.VR} \cdot \lambda_R \cdot V_{Rd} \tag{B7}$$

$$\mu_E \approx \mu_{\theta.MR} \cdot \lambda_E \cdot V_{Ed} \tag{B8}$$

Where λ_R and λ_E are bias factors relating the design values V_{Rd} and V_{Ed} with the values of shear resistance and shear force calculated with the mean values of material and geometrical properties and without partial factors for materials. The bias factors take into consideration the effects of the uncertainties related to the geometrical and material properties and can be calculated with Eq. (B9) and Eq. (B10). For the studied specimens, the bias factors were found to be approximately equal to $\lambda_{R.c}$ = 1.28 and $\lambda_{E.c}$ = 1.17 for members without stirrups; and $\lambda_{R.s}$ = 1.15 and $\lambda_{E.s}$ = 1.17 for members with stirrups. The factors $\mu_{\theta.VR}$ and $\mu_{\theta.MR}$ are the mean values of the model uncertainty for shear and moment capacity.

$$\lambda_R = \frac{V_{Rm}}{V_{Rd}} = \frac{V_R(f_{cm}, f_{ym}, d_m, \gamma_c = 1.0, \gamma_s = 1.0)}{V_R(f_{ck}, f_{yk}, d_k, \gamma_c = 1.2, \gamma_s = 1.0)} \tag{B9}$$

$$\lambda_E = \frac{V_{Em}}{V_{Ed}} = \frac{V_E(f_{cm}, f_{ym}, d_m, \gamma_c = 1.0, \gamma_s = 1.0)}{V_E(f_{ck}, f_{yk}, d_k, \gamma_c = 1.2, \gamma_s = 1.0)} \tag{B10}$$

Inserting (B7) and (B8) into Eq. (B5) yields:

$$\mu_{\theta.VR} \cdot \lambda_R \cdot V_{Rd} \geq \gamma_G \cdot \mu_{\theta.MR} \cdot \lambda_E \cdot V_{Ed} \tag{B11}$$

$$V_{Rd} \geq \gamma_G \cdot \frac{\mu_{\theta.MR} \cdot \lambda_E}{\mu_{\theta.VR} \cdot \lambda_R} \cdot V_{Ed} \tag{B12}$$

An expression for $\gamma_V(\beta)$ can then be derived by comparison with Eq. (4.5):

$$\gamma_V(\beta) = \frac{\mu_{\theta.MR} \cdot \lambda_E}{\mu_{\theta.VR} \cdot \lambda_R} \cdot \gamma_G \approx \frac{\mu_{\theta.MR} \cdot \lambda_E}{\mu_{\theta.VR} \cdot \lambda_R} \cdot e^{(-\alpha_E \cdot CoV_E + \alpha_R \cdot CoV_R) \cdot \beta} \tag{B13}$$

The coefficient of variation of *R* and *E* can be estimated based on the coefficient of variation for the model uncertainties and relevant material and geometrical properties, as given by the following expressions:

$$CoV_{R.Vc} = \sqrt{CoV_{\theta.RVc}{}^2 + \frac{1}{9} COV_{f.c}{}^2} \tag{B14}$$

$$CoV_{R.Vs} = \sqrt{CoV_{\theta.RVs}{}^2 + COV_{f.y}{}^2 + COV_d{}^2} \tag{B15}$$

$$CoV_E = \sqrt{CoV_{\theta.M}{}^2 + COV_{f.y}{}^2 + COV_d{}^2} \tag{B16}$$